**Atmospheric
Chemistry
and Physics**

Multi-scale model analysis of boundary layer ozone over East Asia

M. Lin[1], T. Holloway[1], T. Oki[2], D. G. Streets[3], and A. Richter[4]

[1]Center for Sustainability and the Global Environment, Nelson Institute for Environmental Studies,
University of Wisconsin-Madison, Madison, WI, USA
[2]Institute of Industrial Science, University of Tokyo, Tokyo, Japan
[3]Argonne National Laboratory, Argonne, IL, USA
[4]Institute of Environmental Physics, University of Bremen, Bremen, Germany

Abstract. This study employs the regional Community Multiscale Air Quality (CMAQ) model to examine seasonal and diurnal variations of boundary layer ozone (O_3) over East Asia. We evaluate the response of model simulations of boundary layer O_3 to the choice of chemical mechanisms, meteorological fields, boundary conditions, and model resolutions. Data obtained from surface stations, aircraft measurements, and satellites are used to advance understanding of O_3 chemistry and mechanisms over East Asia and evaluate how well the model represents the observed features. Satellite measurements and model simulations of summertime rainfall are used to assess the impact of the Asian monsoon on O_3 production. Our results suggest that summertime O_3 over Central Eastern China is highly sensitive to cloud cover and monsoonal rainfall over this region. Thus, accurate simulation of the East Asia summer monsoon is critical to model analysis of atmospheric chemistry over China. Examination of hourly summertime O_3 mixing ratios from sites in Japan confirms the important role of diurnal boundary layer fluctuations in controlling ground-level O_3. By comparing five different model configurations with observations at six sites, the specific mechanisms responsible for model behavior are identified and discussed. In particular, vertical mixing, urban chemistry, and dry deposition depending on boundary layer height strongly affect model ability to capture observed behavior. Central Eastern China appears to be the most sensitive region in our study to the choice of chemical mechanisms. Evaluation with TRACE-P aircraft measurements reveals that neither the CB4 nor the SAPRC99 mechanisms consistently capture observed behavior of key photochemical oxidants in springtime. However, our analysis finds that SAPRC99 performs somewhat better in simulating mixing ratios of H_2O_2 (hydrogen peroxide) and PAN (peroxyacetyl nitrate) at flight altitudes below 1 km. The high level of uncertainty associated with O_3 production in Central Eastern China poses a major problem for regional air quality management. This highly polluted, densely populated region would greatly benefit from comprehensive air quality monitoring and the development of model chemical mechanisms appropriate to this unique atmospheric environment.

1 Introduction

Ozone (O_3) is a secondary pollutant produced in the troposphere by photochemical oxidation of volatile organic compounds (VOCs) and carbon monoxide (CO) in the presence of nitrogen oxides ($NO_x=NO+NO_2$). Ozone may also be transported from the stratosphere to the troposphere. Ground-level O_3 is a major component of urban smog that poses a significant risk for public health, and O_3 throughout the troposphere is an important greenhouse gas (Fishman et al., 1979). Ozonesonde observations in Japan (Naja and Akimoto, 2004) and Hong Kong (Liu et al., 2002) show that the seasonal cycle of O_3 in the boundary layer has a broad summer minimum at lower latitudes of the Asian Pacific Rim, in contrast to summer maximums observed at regionally polluted sites in North America and Europe (Jacob, 1999). Recent studies over Eastern China report that surface O_3 exhibits a narrow peak in early summer (May or June) and a sharp drop in July and August, based on measurements

Correspondence to: M. Lin
(mlin26@wisc.edu)

taken in downwind of Beijing (Ding et al., 2008; Wang et al., 2008; Lin et al., 2008c), at three mountaintop sites (Li et al., 2007), and at a rural site near Shanghai (Xu et al., 2008). Previous studies have suggested that the East Asia monsoon is responsible for the observed summer minimum of boundary layer O_3 along the west Pacific coast (Liu et al., 2002; He et al., 2008, and references therein). However, a distinctly different seasonal pattern of surface O_3 with a broad summertime maximum during May–August is observed at Mt. Waliguan (3.8 km above sea level), located on the northeastern edge of the Tibetan Plateau. Meteorological simulations (Ding and Wang, 2006) and regional model analysis from tagged emission sources (Ma et al., 2002, 2005) suggest that the episodic elevated surface O_3 mixing ratios at Waliguan are mostly caused by the downward transport of stratospheric air, rather than transport of anthropogenic pollution from Eastern China (Zhu et al., 2004). Current understanding of the spatial and temporal variations of tropospheric O_3 in China is far from complete. More detailed model analysis is needed to interpret the observed features of tropospheric O_3 over this rapidly growing economic region.

Accurate prediction of tropospheric O_3 presents a particular challenge in chemical transport models (CTMs) due to the complex physical and chemical processes occurring from global to local scales. A number of regional CTMs have been employed to study episodic chemical transport and transformations of Asian pollutants in springtime (e.g. Carmichael et al., 2003c; Zhang et al., 2003; Wang et al., 2006), and the seasonal cycle of surface O_3 in Eastern China (Li et al., 2007) and Japan (Yamaji et al., 2006). Results from the MICS-Asia regional model intercomparison study found that O_3 predictions for July over Central Eastern China differ by ∼20 ppbv among seven regional CTMs (Han et al., 2007). This divergence in model estimates suggests that important questions remain on the key mechanisms controlling the O_3 budget over East Asia. Chemical mechanisms have been found to substantially impact model predictions of O_3 over North America, and the effects of NO_x and VOCs emissions controls vary depending on chemistry (e.g., Sarwar et al., 2008; Luecken et al., 2007; Arnold and Dennis, 2006). However, the response of local and regional O_3 in Asia to choice and implementation of chemical mechanisms has not been evaluated yet. Several studies have addressed the significant impact of the Asian monsoon on O_3 production over Eastern China (He et al., 2008; Wang et al., 2008), but evaluation of how well meteorological models can reproduce monsoon rainfall and its implication on O_3 prediction is insufficient.

This study employs the regional Community Multiscale Air Quality (CMAQ v. 4.6) model (Byun and Ching, 1999; Byun and Schere, 2006) to examine seasonal and diurnal variations of boundary layer O_3 over East Asia. The CMAQ model is driven by MM5 and by WRF meteorological fields. Chemical boundary conditions for CMAQ are derived from the global Model for Ozone and Related Tracers (MOZART v. 2.4) (Horowitz et al., 2003). This is a contemporary

model set-up, and there are not many results presented yet for East Asia. The purpose of this paper is to provide a first step in evaluating the response of model simulations of local and regional O_3 in Asia to the choice of chemical mechanisms, meteorological fields, boundary conditions, and model resolutions. From this analysis, we examine key mechanisms controlling boundary layer O_3 over East Asia, discuss the reasons for discrepancies between model results and observations, and make recommendations regarding optimal regional-scale model configurations for future studies of East Asian O_3 prediction. Section 2 gives an overview of observational data and model configurations. Discussion of O_3 seasonality is presented in Sect. 3. We first examine the impacts of global pollution inflow, the Asian monsoon, and photochemistry on the seasonal cycle of surface O_3 at ground-based stations in Siberia, Japan, China, and Southeast Asia. Satellite data and model simulations of precipitation and tropospheric NO_2 columns are used to help interpret seasonal behavior of boundary layer O_3. Then, with a focus on the spring and summer seasons, Sect. 4 analyzes major photochemical products using two widely used chemical schemes and compares model results with aircraft measurements. Section 5 presents the diurnal variability of summertime ground-level O_3. We examine the impacts of boundary layer mixing, local chemistry, and dry deposition processes on the formation of ground-level O_3.

2 Models and data

2.1 Meteorological fields

We tested the CMAQ model with three sets of meteorological fields for 2001. Table 1 gives horizontal scales, vertical layers, large-scale meteorological fields and physical parameterizations employed for the meteorological simulations. CMAQ was initially driven with meteorological fields from MM5 on an 81×81 km^2 primary domain over East Asia and on a 27×27 km^2 nested domain over Northeast Asia (hereafter referred to as MM5-CMAQ) (Fig. 1a). Vertical layer collapsing was performed to generate eight-layer meteorological fields for CMAQ. Similar configurations of MM5-CMAQ were successfully employed to study long-range transport of acidifying substances over East Asia, and results were presented in Lin et al. (2008a) for model evaluation and in Lin et al. (2008b) for estimating source-receptor relationships. The reader is referred to Lin et al. (2008a) for a detailed description of emissions data and its processing. To examine if vertical layer collapsing would undermine model performance for O_3 predictions, we employ the Weather Research and Forecasting (WRF) model with higher vertical resolution as an alternative meteorological model for CMAQ (hereafter referred to as WRF-CMAQ). The WRF-CMAQ simulation includes 29 vertical layers extending from 8 m to 20 km above ground, with eleven layers in the lowest

Table 1. Model configurations

Configurations	Domain 1 (D1)	Domain 2 (D2)	Domain 3 (D3)
Meteorology model	MM5	MM5	WRF
Horizontal resolution	81 km	27 km	27 km
Met. vertical layers	23 (8 in lowest 2 km)	23 (8 in lowest 2 km)	29 (11 in lowest 2 km)
Depth of first model layer	73 m	73 m	17 m
Model top	100 hPa	100 hPa	50 hPa
Land surface model	NOAH	NOAH	NOAH
Global analysis	NCEP/NCAR ($2.5 \times 2.5°$, 6 h)	NCEP/NCAR	FNL ($1 \times 1°$, 6 h)
Boundary layer scheme	MRF	MRF	YSU
Microphysics	REISNER1	REISNER1	WSM-6
Longwave radiation	Cloud	Cloud	RRTM
Cumulus parameterization	Grell scheme	Grell scheme	Kain-Fritsch scheme
Analysis nudging	Yes	Yes	Yes
Met initialization[a]	Continuous run	Continuous run	Re-initialize every 5.5 days
CMAQ vertical resolution	8 (5 in lowest 2 km)	8 (5 in lowest 2 km)	Same as WRF
CMAQ boundary condition	MOZART (monthly)	CMAQ D1 (hourly)	MOZART[b]

a Data for initial twelve hours are not used by CMAQ to allow the spin up of clouds and other climate processes.
b WRF-CMAQ uses dynamic hourly BC for March, and monthly mean BC for JJA.

2 km. The depth of the first WRF-CMAQ layer is set to 17 m. The vertical resolution of WRF-CMAQ should be fine enough to simulate surface inversion and land-surface interactions. WRF-CMAQ is run for March and summer months (JJA) only, on a 27×27 km^2 domain shown in Fig. 1b. Both MM5 and WRF simulations apply three-dimensional grid nudging towards global analysis. The impacts of meteorological fields on O$_3$ predictions are discussed in both Sect. 3 and 5.

2.2 Gas phase chemistry

In the interest of evaluating model sensitivities to photochemical schemes, we have tested two widely used chemical mechanisms, the Carbon Bond IV (CB4) mechanism (Gery et al., 1989) and the Statewide Air Pollution Research Center (SAPRC99) mechanism (Carter, 2000). The speciation of VOCs to the mechanism-dependent species of CB4 and SAPRC99 is based on a new emission processing model as described in Lin et al. (2008a). CB4 is a lumped-structure condensed mechanism in which organic species are categorized according to reactions of similar carbon bonds (C-C, C=C, C-CHO etc.). The CB4 mechanism in CMAQ contains 36 species and 93 reactions including 11 photolytic reactions. Compared with CB4, SAPRC99 includes more detailed organic chemistry, explicit organic peroxy radicals, and more complete organic intermediates, and provides better representation of peroxides for low NO$_x$ conditions. The SAPRC99 mechanism has assignments for 400 types of VOCs, and can be used to estimate reactivities for 550 VOC categories (Carter, 2000). A total of 24 model species are used to represent the reactive organic product species: 11 are

explicit, and 13 represent groups of similar oxidation reactivity and emission magnitudes using the lumped molecule approach. The SAPRC99 mechanism in CMAQ includes 72 species and 214 reactions including 30 photolytic reactions.

2.3 Boundary conditions

Treatment of lateral and top boundary conditions (BCs) of chemical species is one of the major factors affecting regional model results, especially for long-lived species such as O$_3$, PAN, and CO etc. Most regional models do not apply chemical top BCs, nor does the CMAQ model. Thus, we restrict our comments here to the lateral BCs. CMAQ was initially developed for regulatory purposes, where ground-level pollution is of greatest concern, and numerous evaluations with ground-based measurements have been carried out. For most studies focusing on boundary layer pollution, vertical layer collapsing in the upper troposphere is generally performed to alleviate computational costs (e.g. Arnold and Dennis, 2006; Lin et al., 2008a; Han et al., 2007; Fan et al., 2005). The coarse vertical resolution in the upper troposphere might not resolve the tropopause. When realistic O$_3$ profiles derived from global models or ozonesondes are provided at the model boundaries, O$_3$ in the stratosphere will be quickly dispersed throughout the very thick CMAQ layer that straddles the tropopause, resulting in an artificial downward transport of O$_3$ into the upper troposphere and further to the surface. For this problem, we do not interpolate O$_3$ inflow from the MOZART global model across the tropopause for the annual simulation of MM5-CMAQ with only three layers above 2 km. WRF-CMAQ has adequate vertical resolution in the upper troposphere and lower stratosphere. Sensitivity

Table 2. Ground-based measurement data used in this study.

Name	Type	LAT	LONG	HT (m a.s.l.)	Periods	References
Mondy	Remote	51.67	101.00	2000	2001–2007	P. Pochanart, personal communication (2009), EANET
Beijing	Rural	39–42	115.5–118.5	600	1995–2005[a]	Ding et al. (2008)
Mt. Hua	Mountain	34.49	110.09	2064	2004–2005	Li et al. (2007)
Mt. Tai	Mountain	36.25	117.10	1533	2004–2005	Li et al. (2007)
Mt. Huang	Mountain	30.13	118.15	1836	2004–2005	Li et al. (2007)
LinAn	Rural	30.30	119.73	132	1999–2001[b]	T. Wang, personal communication (2009)
Pohang	Remote	36.00	129.00	–	1995–2000	Kim et al. (2006)
Rishiri	Remote	45.12	141.23	40	2001–2007	EANET (2002–2008)
Tappi	Remote	41.25	141.35	105	2001–2007	EANET (2002–2008)
Sado-seki	Remote	38.25	138.40	110	2001–2007	EANET (2002–2008)
Happo	Remote	36.68	137.80	1850	2001–2007	EANET (2002–2008)
Ijira	Rural	35.57	136.70	140	2001–2007	EANET (2002–2008)
Oki	Remote	36.28	133.18	90	2001–2007	EANET (2002–2008)
Yusuhara	Remote	32.73	132.98	225	2001–2007	EANET (2002–2008)
Hedo	Remote	26.78	128.23	50	2001–2007	EANET (2002–2008)
Ogasawara	Remote	27.08	142.22	230	2001–2007	EANET (2002–2008)
Mt. Sto. Tomas	Mountain	16.00	120.00	2200	1999–2000	Carmichael et al. (2003a)
Bhubeneswar	Remote	20.25	85.87	24	1999–2001	Carmichael et al. (2003a)

[a] Most MOZAIC data were collected during 1997–1998 and around 2005. No data are available for 2001.

[b] Data in 2001 available for March–May only.

tests with and without stratospheric O_3 imported into the WRF-CMAQ domain were carried out, and results are compared with observations from a DC-8 flight designated to examine the influence of stratospheric intrusion. Unless mentioned in the text, other simulations of WRF-CMAQ do not import stratospheric O_3 at the domain boundaries.

In addition to MOZART BC, we have tested several other options, including monthly mean measurement-adjusted MOZART BC and hourly varying BC from the coarse CMAQ simulation. The simulation of MOZART is driven with NCEP reanalysis meteorology for 2000–2002. The evaluation by Holloway et al. (2007) showed that MOZART tends to overpredict monthly averaged surface O_3 over Japan, except in springtime. The overprediction is particularly significant, up to 40%, in summertime. The summertime overprediction is likely due to the coarse horizontal scale implemented by MOZART, which has limited ability in simulating cloud cover and thus enhances O_3 production due to underpredicted cloud cover. In order to reduce the uncertainties introduced in the import of MOZART-derived BCs, we adjusted the concentration of O_3 at the domain boundaries to correct for MOZART bias over Japan as evaluated in Holloway et al. (2007). The reduction of O_3 inflow, which varies on a monthly basis from 0 to 40%, is plotted in Fig. 2a. Results of MM5-CMAQ simulations with original and adjusted MOZART BCs are compared in Section 3.1. Similar adjust-

ment of MOZART BC is applied for the WRF-CMAQ simulation. Monthly mean BC provides a seasonal perspective, but does not resolve possible episodic signals. The MM5-CMAQ simulation with 27 km resolution uses hourly varying BC extracted from the 81 km simulation of CMAQ to examine how the temporal variation of BCs can influence prediction of O_3 variability.

2.4 Observational data

Ground-based measurement data for O_3 and NO_x in Japan obtained under the EANET (Acid Deposition Monitoring Network in Asia) monitoring program (EANET, 2002–2008), were made available for this study. The NASA TRACE-P (Transport and Chemical Evolution over the Pacific) research campaign from February–April 2001 (Jacob et al., 2003), provides a rich dataset for evaluating model results. We use the 5-min merged data sets of the DC-8 and P-3B flights to examine the difference between the CB4 and SAPRC99 chemical mechanisms in simulating key photochemical products. Figure 1 shows locations of ground-based sites and TRACE-P flight paths. Compared with Japan, there are few long-term measurement sites for O_3 in other Asian countries. To provide general insights in seasonal behavior of surface O_3 in China, we compare model results with measurements reported in recently published
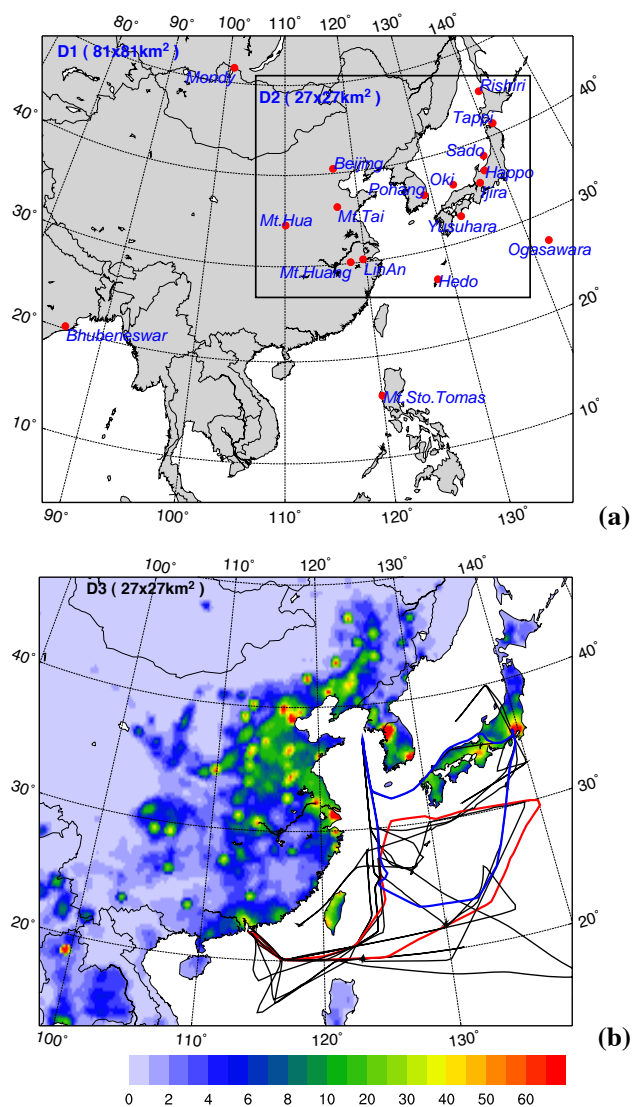
Fig. 1. Model domains: **(a)** MM5-CMAQ domains (D1 and D2) overlayed with ground-based measurement sites. **(b)** WRF-CMAQ domain (D3) overlayed with intensity of NO_x emissions (moles/km^2/h) and flight paths of NASA DC-8 on 7 March (red), 27 March (blue), and other flights (black) during the TRACE-P campaign

research papers (Table 2). Measurement data collected from different research papers might not be for 2001, as it is for the model simulations. In Section 3.2, we discuss inter-annual variability of meteorological conditions and associated impacts on O_3 concentrations.

Three sets of satellite data are used in this study. The TRMM Multi-Satellite Precipitation Analysis (TMPA) (Huffman et al., 2007) is used to evaluate the prediction of the East Asia summer monsoon in MM5 and WRF. The TMPA data (3B43 product, 0.25×0.25°) were provided by the NASA/Goddard Space Flight Center's Laboratory for Atmospheres, which develops and computes the TMPA as a

contribution to TRMM. Satellite data of tropospheric NO_2 columns and fire count are used to help interpret discrepancies between modeled and observed seasonal variations of surface O_3. Tropospheric NO_2 column data (monthly mean, 0.25×0.25°) are based on the GOME (Global Ozone Monitoring Experiment) retrieval by Bremen University (Richter et al., 2005). We sample CMAQ hourly output during GOME overpasses above China (10:30 local time) to calculate monthly mean vertical columns of NO_2 (Lin et al., 2008a). Cloud screening of model results is not applied, and this might introduce a sampling bias between GOME and CMAQ. The total fire count maps are obtained from MODIS (Medium Moderate Resolution Imaging Spectroradiometer) to examine the intensity of biomass burning and its impact on O_3 concentrations.

3 Seasonal cycle of surface ozone

We performed three CMAQ simulations at 81 km horizontal scale with different chemical mechanisms and global BCs, and compared seasonal variations of surface O_3 predictions with ground-based measurements. Measurement sites are classified into three groups representing different seasonal patterns at higher latitudes (Fig. 2a), middle latitudes (Fig. 2b) and lower latitudes (Fig. 2c) in the study domain. The correlation coefficient (R), mean bias (MB), and root mean square error ($RMSE$) are chosen to measure model performance.

3.1 Impacts of boundary conditions

Three ground-based measurement sites (Mondy, Rishiri, and Tappi) close to the northern boundary of the model domain are chosen to diagnose the impacts of global pollution inflow. The comparison between two SAPRC99 simulations with original and controlled MOZART BC demonstrates that adjusting O_3 inflow from the global model reduces the mean bias by ∼5 ppbv on seasonal predictions at these three sites. CMAQ predictions at Mondy with adjusted O_3 inflow show root mean square error ($RMSE$) of 1.7 ppbv as compared to $RMSE$=7.4 ppbv with the original MOZART BC. Adjusting the inflow of O_3 pollution exerts a greater influence on wintertime O_3 predictions, reflecting longer lifetime of O_3 in the wintertime atmosphere. Using measurement-adjusted O_3 inflow tends to improve CMAQ's performance in simulating wintertime surface O_3 in Northern (Rishiri and Tappi) and Central Japan (Oki), as compared with measurements.

Evaluation with TRACE-P measurements shows that WRF-CMAQ reproduces well the magnitude and variation of O_3 at flight altitudes below 3 km (Sect. 4.2), however, generally underpredicts O_3 at altitudes above 3 km. Carmichael et al. (2003c) and Han et al. (2007) found a similar pattern with the lowest correlation coefficient for O_3 above 3 km, using other regional models not applying top BCs of chemical
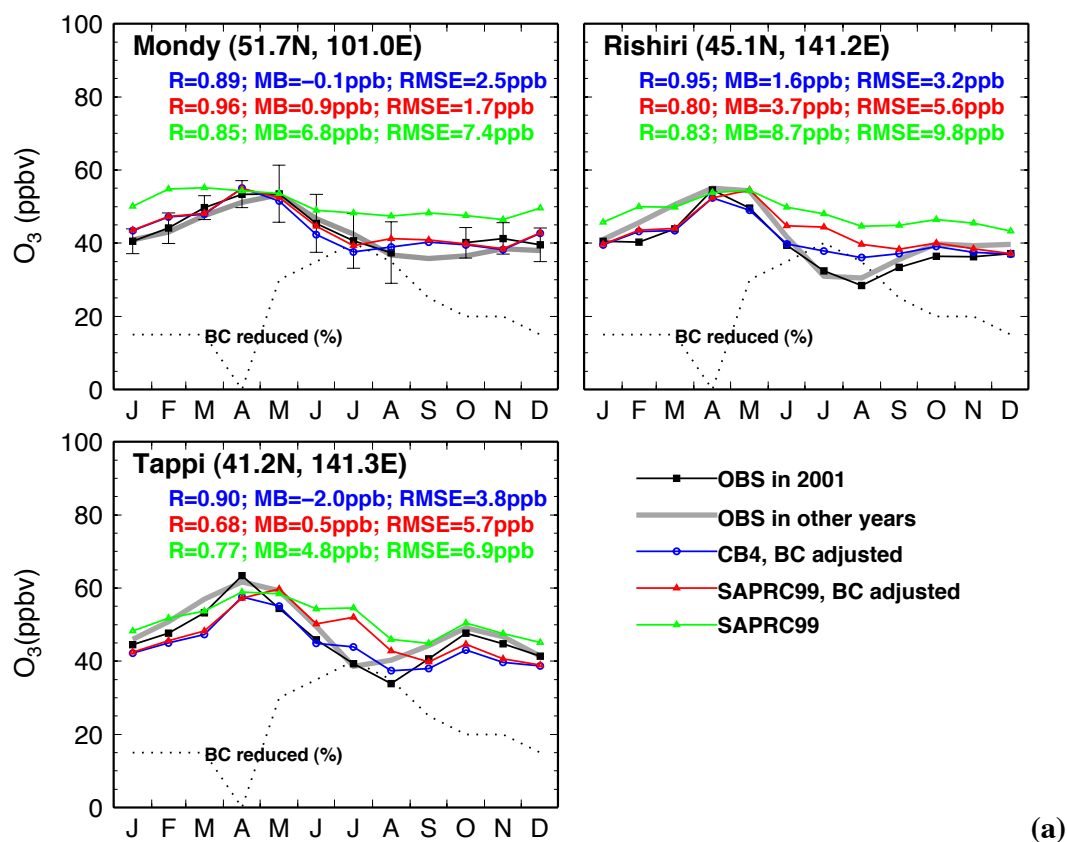
Fig. 2a. Seasonal variations of observed and predicted surface ozone from the MM5-CMAQ simulations with 81 km resolution at **(a)** high-latitude sites, **(b)** mid-latitude sites, and **(c)** low-latitude sites. The dotted line shows the percentage reduction of ozone mixing ratios imported from the MOZART global model at the domain boundaries. The reduction percentage corresponds to the bias between MOZART predictions and measurements over Japan. The whiskers are ± one standard deviation of measurement data for available sites.

species. The DC-8 flight on 27 March during the TRACE-P campaign was intended to examine convective outflow and stratospheric influence. Figure 12 illustrates the comparison of observed and modeled O_3 from WRF-CMAQ with and without stratospheric O_3 imported at the domain boundaries. Ethane distributions along the flight path are also shown. Ethane has simple removal mechanisms in the atmosphere; thus its distributions are mainly controlled by transport and emissions processes. We find that both observed and modeled ethane and NO_x levels are low at ~1 and ~05:00 UTC and variations have a negative correlation with O_3 profiles, suggesting that high-observed O_3 in these periods is not pollution transported from the boundary layer. Instead, the high-observed O_3 at ~10 km reflects the intrusion of stratospheric air. In the period between 04:00 and 06:00 UTC, when the aircraft was at ~10 km, observed O_3 levels are in excess of 150 ppbv. WRF-CMAQ with realistic inflow of stratospheric O_3 at the domain boundaries (green lines in Fig. 12) is able to reproduce the stratospheric-originating O_3 around 05:00 UTC, but still underestimates O_3 around 01:00 UTC. As the need to use global model BC increases, along with the need to apply CMAQ for regions frequently impacted by

stratospheric intrusions, it is becoming apparent that chemical top BCs should be implemented in future versions of CMAQ and other regional models.

3.2 Impacts of East Asia monsoon

The MM5-CMAQ simulations at 81-km horizontal scale (hereafter referred to as MM5-CMAQ/81 km) show a latitudinal difference in reproducing O_3 seasonality, with the best ability at lower-latitude sites (Fig. 2c) and worst at mid-latitude sites (Fig. 2b). Surface O_3 at Mt. Sto. Tomos stays as low as 20–30 ppbv all year long with weak seasonal variability–indicating the seasonal dominance of clean marine air masses. At Hedo and Ogasawara, slightly to the north, surface O_3 exhibits strong seasonal variations with a maximum in winter and spring – transported from continental Asia – and a minimum in summer due to the southwesterly monsoonal intrusion. Impacts of the monsoonal intrusion on O_3 mixing ratios at three island sites at lower latitudes (Mt. Sto. Tomos, Hedo, and Ogasawara) are reasonably well simulated by the model. All simulations successfully reproduce the observed seasonal cycle of surface
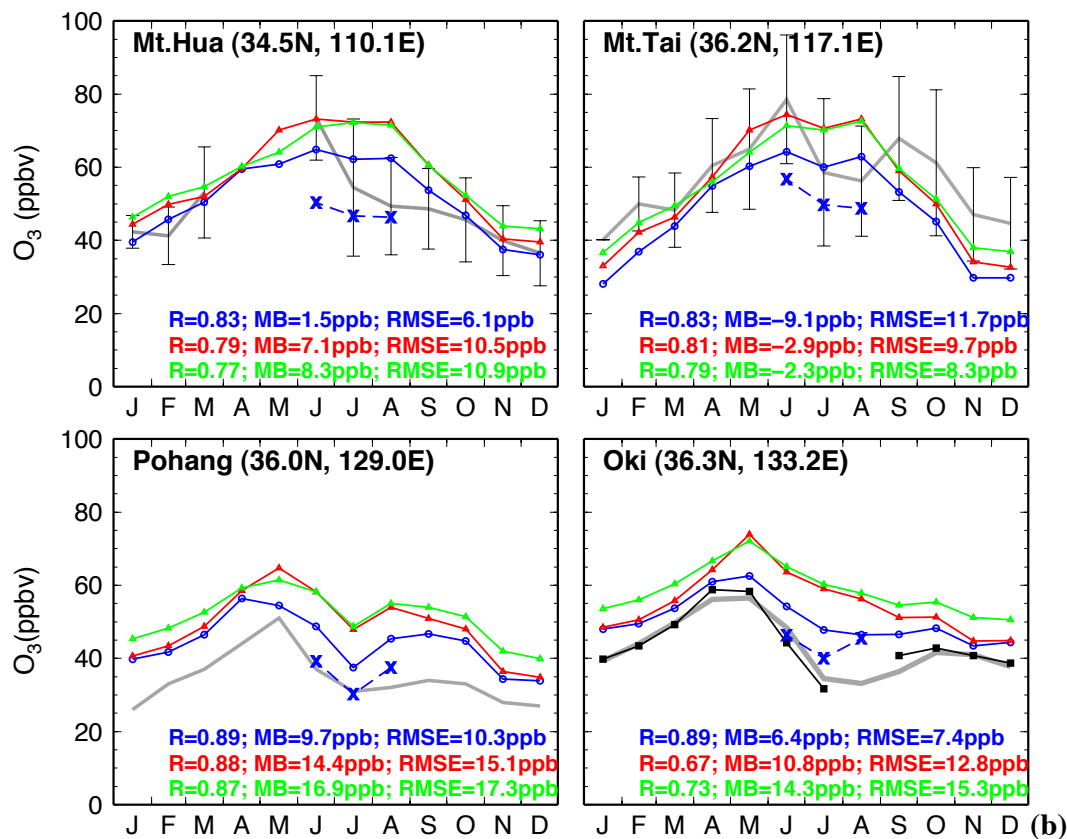
Fig. 2b. Continued. Blue crosses represent model results from the WRF-CMAQ simulation with the CB4 chemistry, which is run for March and June–August 2001 only.

O_3 at Hedo with correlations of R=0.98. The models also show a correlation of R=0.9 at Ogasawara, close to the eastern boundary. An overprediction found at Ogasawara during January–March is likely attributable to the error of O_3 inflow from MOZART, considering that the dominant flow south of 30° N near this site is from the northeast in wintertime.

Compared with the remote island sites, local photochemical production and transport of regionally polluted air tend to have a greater impact on the O_3 budget at the inland Chinese sites. Observed surface O_3 at the rural site Lin'an and at three mountaintop sites (Huang, Tai and Hua) exhibit late spring/early summer maximums and drop to low values in July and August. Compared with the observed seasonal trend of surface O_3, MM5-CMAQ/81 km with CB4 chemistry shows correlations of R=0.7∼0.8 at these sites in Eastern China. The observed peak in late spring and sharp drop in July of surface O_3 at Mt. Huang are well reproduced, but surface O_3 levels in August at all Eastern China sites are overpredicted by MM5-CMAQ/81 km. Especially at Mt. Tai, Mt. Hua and Beijing, model simulations with both gas phase chemistry of CB4 and SAPRC99 do not capture the decrease in observed O_3 in July and August relative to June. Overprediction of July and August O_3 over Central Eastern China from the MM5-CMAQ/81km simulation shown in this study

is consistent with results reported for seven regional CTMs (Han et al., 2007) and 21 global CTMs (Fiore et al., 2008) in comparison to EANET data from Japan. Wang et al. (2008) also found that the GEOS-Chem global CTM overestimated July O_3 mixing ratios observed at a rural site near Beijing.

The East Asia summer monsoon has significant impacts on the seasonal behavior of boundary layer O_3 across the Asian Pacific Rim. A recent study using the seasonal and geographical distribution of the monsoon index suggested that the East Asia summer monsoon is responsible for the bimodal seasonal O_3 pattern over Central Eastern China (He et al., 2008). The intrusion of low-O_3 marine air masses is the key mechanism contributing to the summer minimum of boundary layer O_3 observed at lower latitudes of the western Pacific (Naja and Akimoto, 2004; Liu et al., 2002). Clouds associated with monsoon rainfall indirectly affect pollutant concentrations by altering solar radiation, which in turn affects the flux of biogenic emissions and photochemical production of O_3. Wang et al. (2008) described that photochemical production of O_3 at a rural site downwind of Beijing is suppressed in the presence of increased cloudiness during July and August associated with the monsoon rainfall, even though CO mixing ratios increase.
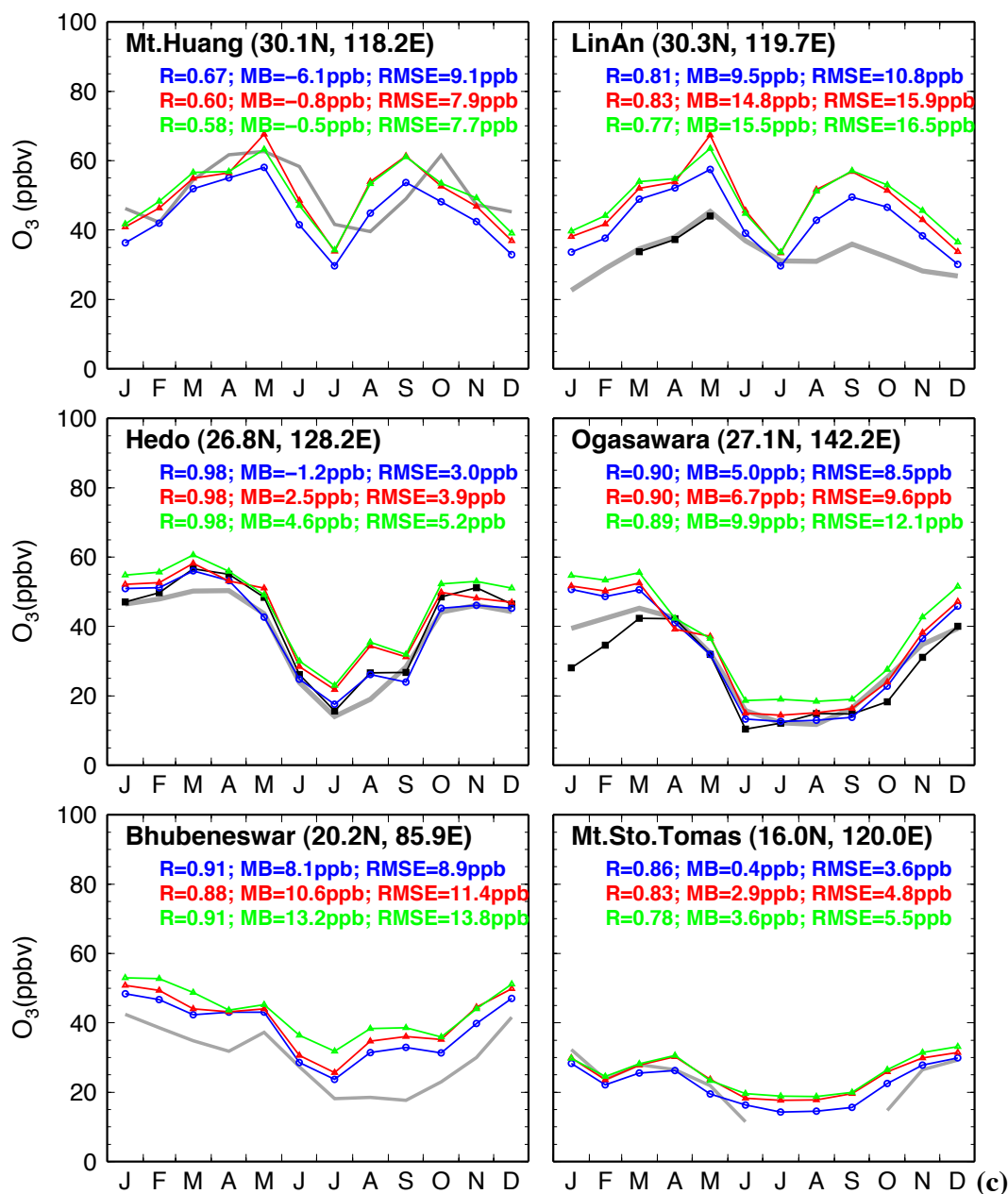
Fig. 2c. Continued.

In light of the significant impacts of the Asian monsoon and associated cloud cover on the summertime O_3 budget over Eastern China, we use the TRMM satellite precipitation analysis to evaluate how well MM5 and WRF can reproduce monsoon rainfall and assess its influence on model prediction of O_3. Figure 4 compares observed and modeled precipitation in June and July 2001. The TRMM satellite measurements reveal that a strong monsoon is developed over Central Eastern China and the Korean Peninsula in July. Central Eastern China in July is affected by southwesterly and southeasterly monsoonal flow, and pollution is then subject to fre-

quent lifting into the upper troposphere by convection (Liu et al., 2002). In June, however, Central Eastern China is under relatively dry conditions. Such intra-seasonal differences in monsoonal rainfall explains the observed decrease in surface O_3 from June to July at a few measurement sites in this region. Both MM5 and WRF capture the increased rainfall over Central Eastern China in July relative to June, but the intensity of monsoonal rainfall over this region in both models is much weaker than that seen from satellites. The MM5 simulation at 81 km horizontal scale also significantly underpredicts TRMM rainfall over south China in both June and
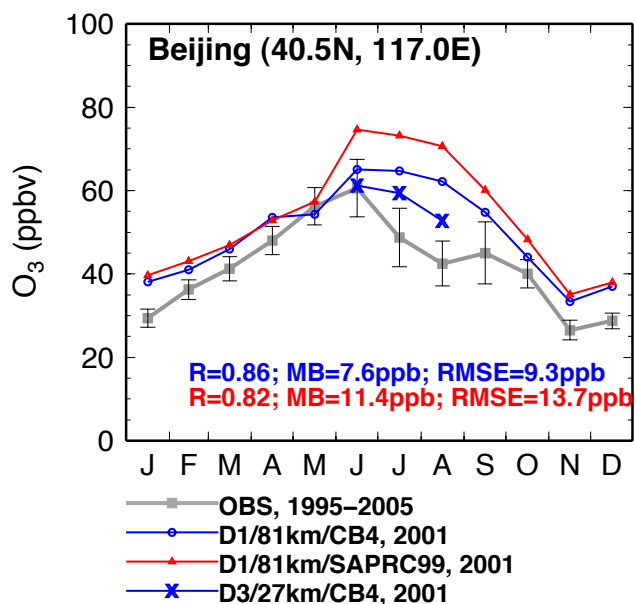
Fig. 3. Observed and simulated seasonal cycle of daytime (05:00 a.m.–04:00 p.m.) ozone over Beijing. The whiskers are ± one standard deviation of measurement data.

July. Relative to MM5, the WRF simulation at 27 km horizontal scale reproduces well both the magnitude and spatial distribution of TRMM rainfall over South China. The distinct difference in simulating monsoonal rainfall between MM5 and WRF can be attributed to differences in physical parameterizations (Table 1), model resolution, and the initialization process. The MM5 simulation was initialized with the NCEP/NCAR reanalysis at the beginning of the study period and run continuously throughout the year. Considering the cumulative errors of meteorological models, we reinitialize the WRF model every 5.5 days with FNL analysis to maximize the consistency with large-scale observational data ingested in FNL. Similar reinitialization processes have been applied in other modeling studies (e.g. Tang et al., 2007; Ding and Wang, 2006). The underestimate of monsoonal rainfall in MM5 is primarily due to the cumulative errors of a long-term simulation and the inability of the model's coarse-resolution to simulate cloud cover.

Clouds have significant radiative effects on the photochemistry of O_3 production near the surface (Lefer et al., 2003; Liu et al., 2006). Transmission of solar radiation is reduced below cloud level, thus photochemical production of O_3 is suppressed in the presence of increased cloudiness associated with the monsoon rainfall. Monsoon rainfall also removes soluble O_3 precursors from the atmosphere. In response to reduced cloudiness and monsoon rainfall, MM5-CMAQ produces 10–15 ppbv higher O_3 over Central Eastern China than WRF-CMAQ. The MM5-CMAQ overestimate of surface O_3 at inland Chinese sites relates primarily to the underestimate of monsoonal rainfall and cloud cover, as well as coarse vertical resolution in which strong surface

inversions might not be adequately developed. With the improved meteorological fields from WRF, CMAQ simulates a 10–20 ppbv decrease in O_3 mixing ratios at Mt. Hua and Mt. Tai during June–Augsut, and WRF-CMAQ results with CB4 chemistry are even lower than the observed values (Fig. 2b). For Beijing, the decrease in O_3 mixing ratios in August relative to June is captured by WRF-CMAQ, but the magnitude of low-observed O_3 during July and August is still overpredicted (Fig. 3). Figure 4 shows that WRF predicts less than 2 mm/day rainfall in July over the Beijing surrounding region – which is approximately 50% lower than the TRMM satellite analysis. TRMM estimates 3–5 mm/day rainfall in July over Beijing, consistent with rain gauge records reported in Ding et al. (2008). The unrealistic dry and less cloudy conditions in the model promotes O_3 production over this region. Our analysis confirms that systematic overprediction of summertime O_3 found in both regional and global CTMs is due to model inability to accurately simulate cloud cover and monsoon rainfall and inadequate representation of southwesterly/southeasterly inflow of marine air masses in the global meteorological reanalysis data.

It should be noted that model results are for 2001 while measurement data at three mountaintop sites (Mt. Tai, Mt. Hua, and Mt. Huang) are for March 2004–February 2005 (Li et al., 2007), and the MOZAIC aircraft observations for Beijing are the average of data mostly collected during 1997–1998 and around 2005 (Ding et al., 2008). Our analysis of NCEP/NCAR winds and geopotential heights shows that the general transport pattern in 2001 is similar to the climatology over 1980–2005 even though a slightly different pattern is found in August. Figure 5 compares the climatological pattern of NCEP/NCAR winds and geopotential fields at 850 hPa in August for 1980–2005 with those for 2001. The Western North Pacific (WNP) anticyclone plays an important role in the connection between the East Asia summer monsoon and the tropical sea surface temperature anomalies (e.g. Lee et al., 2008), and is characterized by southwesterly airflow along the east Asian coast. We find that in August 2001 the WNP anticyclone moved to the northeast as compared with the climatological pattern. 2001 is also found to be a weak La Niña year. The distributions of geopotential height in Fig. 5 indicate that there is a localized high pressure system over Central Eastern China in August 2001. The relatively high geopotential height over Central Eastern China suggests a weakened monsoon in the same region. Supporting this conclusion, TRMM detected that the precipitation amount over Central Eastern China in August 2001 is 2 mm/day on average lower than the climatological mean. Comparison of 2001 O_3 measurements and average values during 2001–2007 at the EANET sites shows that the general pattern of the O_3 seasonal cycle did not change for 2001 at the Japanese sites (Fig. 2). For August, we find that the Hedo site located on Okinawa island recorded 8 ppbv higher O_3 in 2001 than the average during 2001–2007, and TRMM detected 3 mm/day lower precipitation over the island. Our
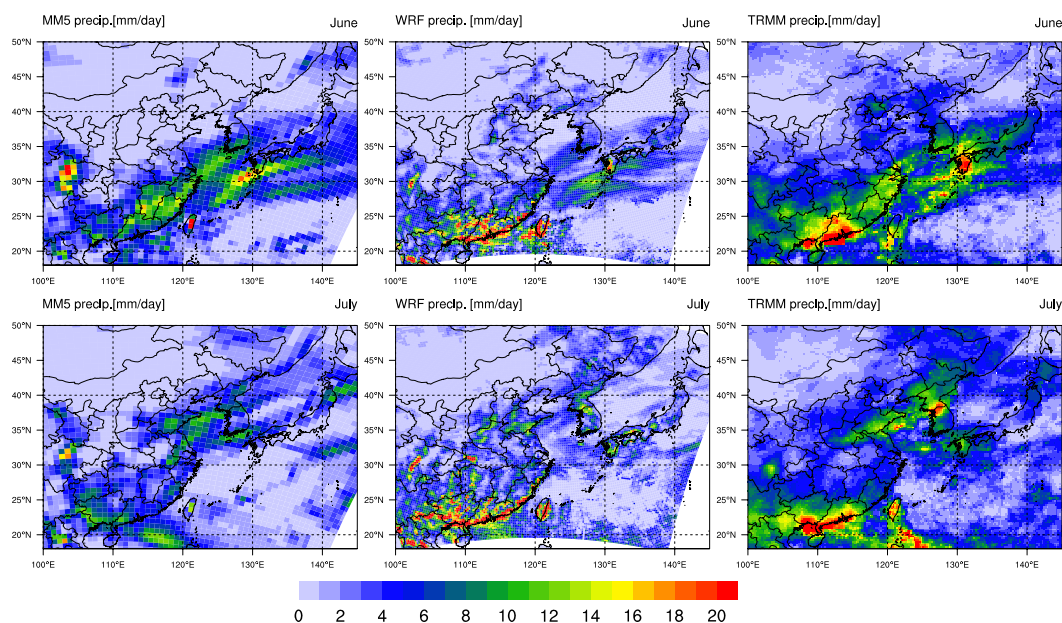
Fig. 4. Comparison of observed and modeled precipitation in June and July 2001.

analysis suggests that the weakened summer monsoon over Central Eastern China in August 2001 might contribute to O_3 enhancement over this region, but the impact is likely lower than 5–10 ppbv.

3.3 Ozone June maximum over Central Eastern China

Boundary layer O_3 over Central Eastern China appears to reach its seasonal maximum in June. Modeled afternoon (12:00 p.m.–06:00 p.m.) O_3 in June shows a typical spatial pattern with low mixing ratios south of 30° N and a region of O_3 greater than 50 ppbv stretching across northern China (Fig. 6). The high-O_3 enhancement across northern China coincides with the region of relatively low precipitation as revealed in meteorological model simulations and TRMM satellite measurements. Elevated O_3 over the Yellow Sea reflects significant contributions of northeastward offshore transport of aged and polluted air across the water (higher production of OH via $O(^1D) + H_2O \rightarrow 2OH$) and the effects of the marine boundary layer. The marine boundary layer suppresses ventilation of surface pollutants as well as reduces dry deposition velocities since marine boundary layer processes, in general, are less turbulent than their counterparts over land. Beijing and its surrounding region exhibit typical O_3 mixing ratios in excess of 75 ppbv – the US EPA air quality standard of 8-h O_3.

Evaluation with TRMM satellite measurements demonstrates that the WRF model generally captures intra-seasonal differences in monsoon rainfall during June, July and August 2001. With the improved meteorological fields from WRF, we find that CMAQ largely underpredicts the observed June O_3 maxima at Mt. Hua and Mt. Tai (Fig. 2b). To examine if there are additional emission sources in June missing in the model, we compared model estimates of tropospheric NO_2 columns with GOME observations (Fig. 7). The comparison reveals that a relatively strong signal of GOME NO_2 columns over Central Eastern China in June is not seen in the model, even though the magnitude of GOME NO_2 in July and August over most areas is reasonably reproduced. We have also examined NO_2 satellite data from more recent instruments (SCIAMACHY, GOME-2, and OMI) and found similar patterns in other years with greater June NO_2 over Central Eastern China. The seasonal variation of atmospheric NO_2 is mainly determined by the changing sunlight hours over the year, which affect the dominant sink of NO_2 through reaction with the hydroxyl radical. NO_2 tends to have a shorter lifetime in June relative to rainy/cloudy July and August; thus the difference in lifetime can not explain the stronger signal of GOME NO_2 columns in June. We find that the spatial extents of these high NO_2 features coincide with local fire activity in June 2001 as detected by MODIS (Fig. 8). Fu et al. (2007) found a similar feature in the GOME HCHO column and suggested that the observed high HCHO columns in June are produced by crop residue burning after the harvest of winter wheat. Additional emissions from agricultural burning over Central Eastern China, combined with the pre-summer monsoon conditions, would explain the observed relatively high values of O_3 mixing ratios, GOME NO_2 and HCHO columns in June.

The 81-km run of MM5-CMAQ uses biomass burning emissions data for 2000 from the GEIA/RETRO database (http://www.aero.jussieu.fr/projet/ACCENT/RETRO.php). A recent Global Fire Emission Database (GFED) with inter-annual variations (van der Werf et al., 2006) shows

850hPa August 2001

850hPa August 1980−2005
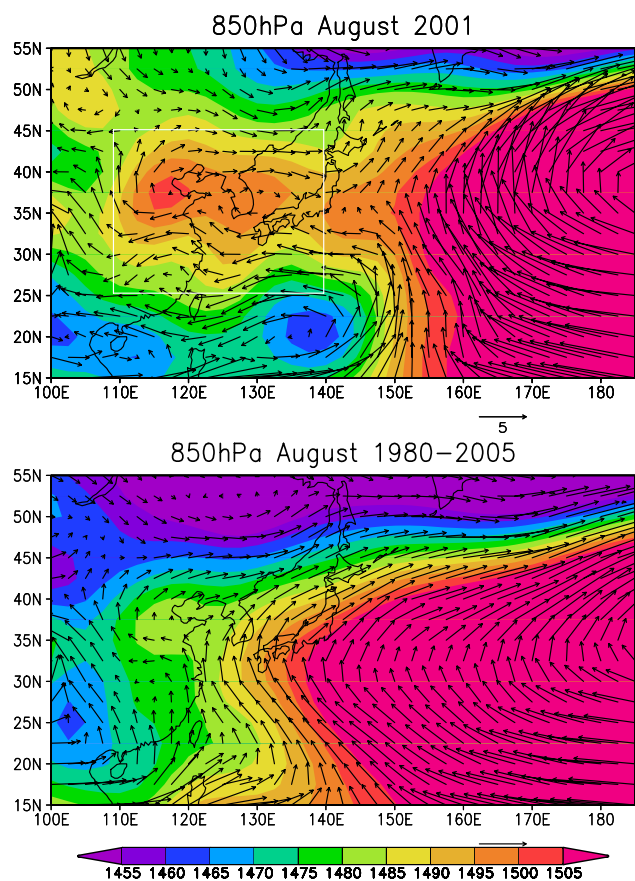
Fig. 5. Monthly mean wind vectors (m/s) and geopotential heights (gpm) at 850 hPa in August for 2001 and the climatological mean during 1980–2005.

that the intensity and spatial distribution of biomass burning emissions are similar between June 2001 and 2004, but weaker in June 2000. We have tested the WRF-CMAQ run using GFED fire emissions for June 2001 and found that GFED fire emissions do not fully account for the strong NO_2 signal from GOME. The magnitude of observed high O_3 at Mt. Tai and Mt. Hua in June is still underpredicted by the CMAQ simulation using GFED fire emissions. There is increasing evidence that VOC emissions over Central Eastern China are underestimated by the current bottom-up emission inventories. Fu et al. (2007) used the GOME HCHO columns to constrain reactive VOC emissions over East Asia and found that GOME-inferred VOC emissions are 25% higher for anthropogenic sources and almost 5 times higher for biomass burning emissions than the Streets et al. (2003) inventory. The GOME-inferred biogenic isoprene emissions over Eastern China are 3 times higher than the estimate by Guenther et al. (2006). A recent study by Zhao et al. (2009) showed that the regional chemical transport model (REAM) greatly underestimates the VOC species leading to PAN formation. The GEOS-Chem global model using GOME-constrained VOC emissions drives
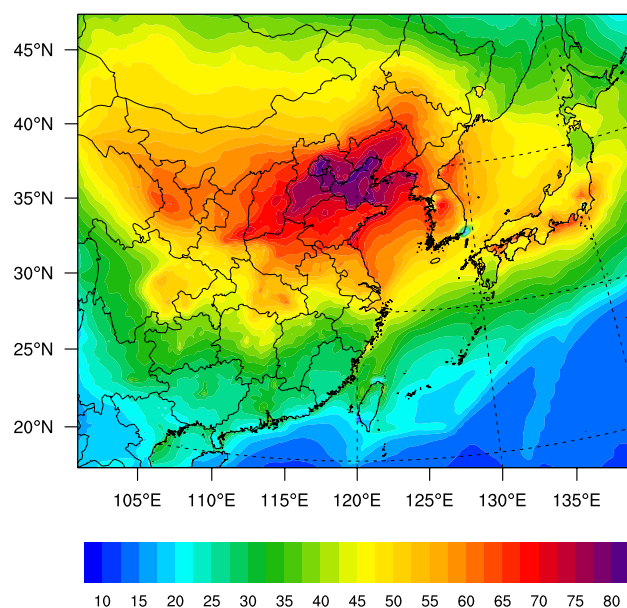

Fig. 6. Predicted afternoon (12:00 p.m.–06:00 p.m.) ozone in ppbv from the WRF-CMAQ simulation for June 2001

a 5–20 ppbv increase in surface O_3 over Central Eastern China relative to using the bottom-up inventories (Fu et al., 2007). Underestimates of VOCs from Eastern China likely explain why CMAQ underpredicts the June maximum of O_3 at Mt. Tai and Mt. Hua as shown in this study. Further sensitivity tests of regional model results with improved emission inventories over China and evaluation with additional ground-based measurements over this region would be extremely valuable in the future.

4 Impacts of chemical schemes

4.1 Spatial and seasonal variations of chemical sensitivity

Examination of modeled O_3 seasonal cycles shows that the difference in surface O_3 is negligible in wintertime between CB4 and SAPRC99 in the MM5-CMAQ/81 km simulations, but is ~10 ppbv in summertime. This divergence in summertime O_3 predictions between two chemical schemes is particularly pronounced at regionally polluted or downwind sites at mid-latitudes (Figs. 2b and 3). In contrast, photochemistry exerts a much smaller influence at coastal and island sites at lower latitudes (Fig. 2c). Figure 9 illustrates the spatial distribution of differences in simulated monthly mean surface O_3 and PAN in July between SAPRC99 and CB4. SAPRC99 and CB4 show little differences in simulating summertime O_3 south of 30–35°N in East Asia where O_3 production tends to be in the NO_x-limited regime, reflecting the high VOC/NO_x ratios due to large contributions of emissions from biogenic sources in summertime. Ozone
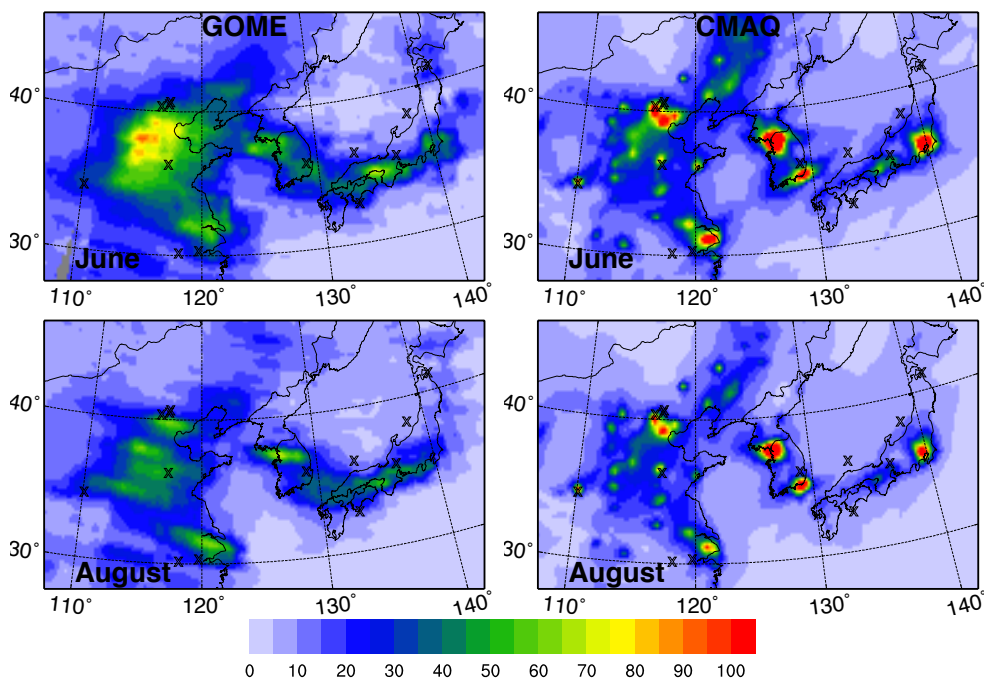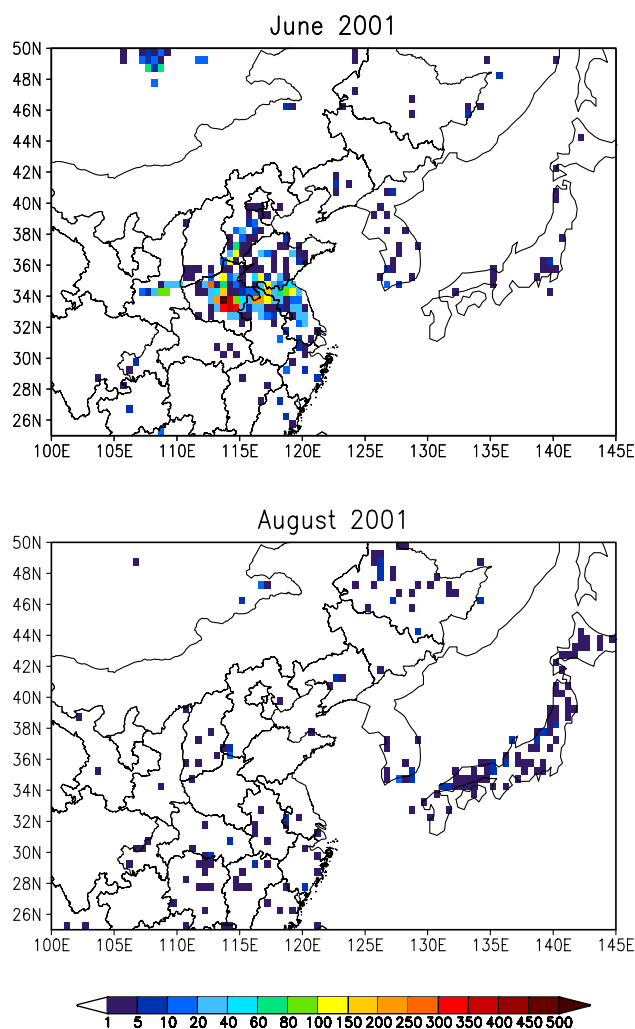
Fig. 7. Tropospheric NO_2 column in 10^{14} molecules cm^{-2} from GOME (left panel) and the WRF-CMAQ simulation (right panel) for June and August of 2001. The CMAQ simulation uses anthropogenic emissions from Streets et al. (2003) and fire emissions from van der Werf et al. (2006). The crosses indicate locations of measurement sites shown in Fig. 1.

formation between 30° N and 45° N across a highly industrialized region in East Asia appears to be most sensitive to the choice of chemical mechanisms. The SAPRC99 mechanism produces 20% higher O_3 and 50–70% more PAN over this polluted region. The high chemical sensitivity indicates that the summertime O_3 budget over this polluted region is dominated by local processes of NO_x-VOC-CO photochemistry. Carmichael et al. (2003c), using a regional model analysis of TRACE-P measurements, suggested that photochemical production of O_3 over Central Eastern China is in the VOC-limited regime during springtime. Zhao et al. (2009), using simulated HCHO/NO_y ratios, inferred that O_3 production over Central Eastern China is less sensitive, relative to other regions of China, to NO_x emissions even though it is still in the NO_x-limited regime in June. Our analysis suggests that O_3 production over Central Eastern China is also highly sensitive to VOC emissions and their reactivities, inferred from higher O_3 yields in SAPRC99 for this region. Prior studies over North America show similar results, with SAPRC99 producing higher O_3 values than CB4 (Arnold and Dennis, 2006; Faraji et al., 2008; Luecken et al., 2007; Yarwood et al., 2003). All of these prior studies have focused on O_3 yields at polluted regions where the O_3 production tends to be in the VOC-limited regime. We show the same tendencies over Central Eastern China where the summertime O_3 budget shows complex interactions among monsoonal flow, regional transport, and local photochemistry. Understanding of O_3 chemistry and mechanisms over this region is far from

complete. Differences in chemical sensitivities give rise to differences in predictions of effects of VOCs and NO_x emissions controls. This poses a particular challenge in choosing a mechanism that best represents regional atmospheric conditions in regulatory applications, for example, designing an emissions control policy for Central Eastern China.

Compared with measurements, MM5-CMAQ/81km with both CB4 and SAPRC99 tends to overpredict summertime O_3 at mid-latitude sites. The CB4 mechanism better reproduces the magnitude of observed summertime O_3 at these sites, however, analysis of satellite measurements and MM5 simulations of monsoonal rainfall presented in the last section, has revealed that CB4 in the MM5-CMAQ simulations actually gives the right answer for the wrong reasons.

Several reasons can explain why SAPRC99 produces higher summertime O_3 over Central Eastern China. From the emissions point of view, total VOC emissions in SAPRC99 should be higher than in CB4, which explains in part why regions in the VOC-limited regime of O_3 production are most sensitive to the choice of chemical mechanisms. SAPRC99 includes a more detailed emission representation of hydrocarbon classification for individual VOC species. Formation of O_3 in SAPRC99 is sensitive to aggregated emissions of highly reactive VOC species. Emission speciation of VOCs, however, may not take full advantage of detailed VOC categories by SAPRC99 since most VOC speciation profiles for Asia are based on the source measurements in North America or Europe. Despite the expected uncertainty

Fig. 8. MODIS total fire count in June and August 2001

mating natural VOC fluxes greatly affects summertime O_3 predictions. Online calculation of biogenic emissions depending on meteorological conditions is recommended for future studies.
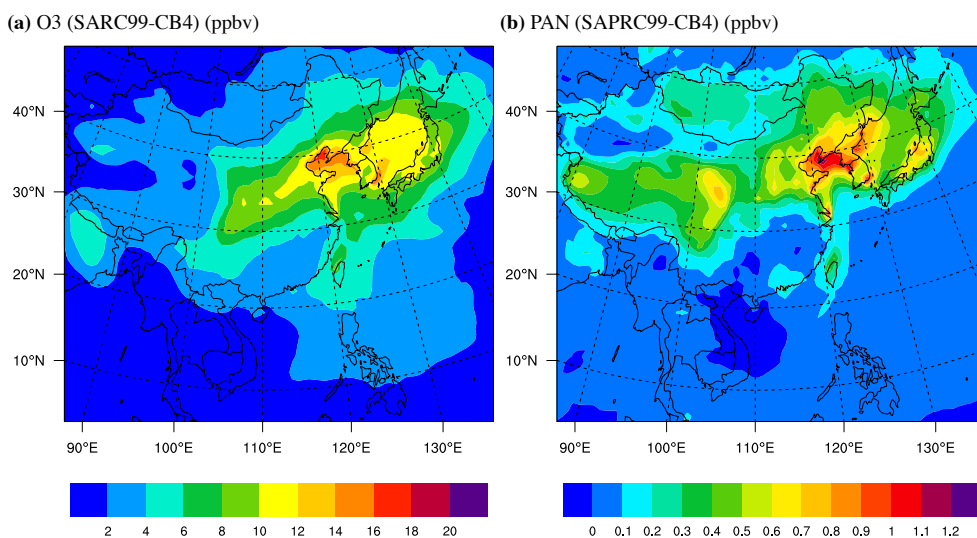
From a chemistry point of view, the newer mechanism SAPRC99 has a better characterization of radical recycling than CB4. With inclusion of radical recycling processes, compounds that were previously considered termination products can re-form reactive species. For example, the rate of the main radical termination process, the reaction of the hydroxyl radical with NO_2 ($OH+NO_2 \rightarrow HNO_3$) is greater in CB4 relative to SAPRC99. In summertime, CB4 produces 10–30% higher nitric acid (HNO_3) that is quickly dry deposited and thus permanently removes a significant fraction of NO_x from the system which otherwise may have been recycled. In addition to the radical recycling process, Faraji et al. (2008) identified aromatic reactions as an important source of differences in O_3 formation between CB4 and SAPRC99. Evaluation of modeled key photochemical species with measurements would provide further insights to photochemical mechanisms in CB4 and SAPRC99. Summertime is found to be the most sensitive season in our study to the choice of chemical mechanisms, however, there is no observational data available to evaluate model results for summertime.

### 4.2 Evaluation with TRACE-P measurements

Measurements of key photochemical species during the TRACE-P campaign for March 2001 provide a unique opportunity to evaluate regional models for Asia. Model results from the WRF-CMAQ simulations were interpolated to the aircraft location and time. Performances of CB4 and SAPRC99 mechanisms in simulating main photochemical oxidants (O_3, PAN, and H_2O_2) and key radicals (OH and HO_2) are compared. Results are shown in Fig. 10 with scatter plots of all DC-8 and P-3B flights in the study region, and in Figs. 11–12 for comparison along the DC-8 flight paths on 7 and 27 March.

SAPRC99 and CB4 show little difference in simulating springtime O_3. Overall both mechanisms reproduce well measured O_3 levels at flight sections below 3 km with correlations of $R \geq 0.75$. We discussed the discrepancy above 3 km in Sect. 3.1. In many flight segments, modeled OH from both mechanisms closely tracked the observed values. However, CB4 tends to predict higher OH levels at some flight sections, such as the DC-8 flight at 02:00 to 04:00 UTC on 7 March (Fig. 11). SAPRC99 shows stronger variability in the OH level along the flight path, reflecting the faster production and termination processes of radicals. Large differences in PAN and H_2O_2 mixing ratios are found between CB4 and SAPRC99 and are discussed below.

Gas-phase PAN is produced via a reversible reaction of the peroxyacetyl radical with NO_2: $CH_3C(O)OO+NO_2 \rightleftharpoons CH_3C(O)OONO_2$. Figure 11 for

in aggregated emissions for individual VOC species, VOC species estimates by Streets et al. (2003) have held up remarkably well in subsequent model and observation comparisons (e.g. Carmichael et al., 2003b). Natural sources of reactive VOCs (especially isoprene and terpenes) are also poorly known. SAPRC99 includes both isoprene and terpene photo-oxidation reactions, while CB4 includes isoprene only and the isoprene chemistry in CB4 is much coarser than in SAPRC99 (Zaveri and Peters, 1999). Isoprene emissions, primarily from oaks and other deciduous trees, exhibit strong seasonal and diurnal variability depending on temperature, solar radiation, Leaf Area Index and plant functional type. Biogenic isoprene plays an important role in contributing to summertime O_3 in many areas. A sensitivity test of CMAQ with SAPRC99 was carried out by removing biogenic emissions, and we find that surface O_3 mixing ratios over Central Eastern China and downwind areas decrease by 10–15 ppbv on average. The results suggest that the uncertainty in esti-

(a) O₃ (SARC99-CB4) (ppbv)

(b) PAN (SAPRC99-CB4) (ppbv)

Fig. 9. Differences in monthly mean surface O_3 and PAN in July 2001 between SAPRC99 and CB4 predictions.
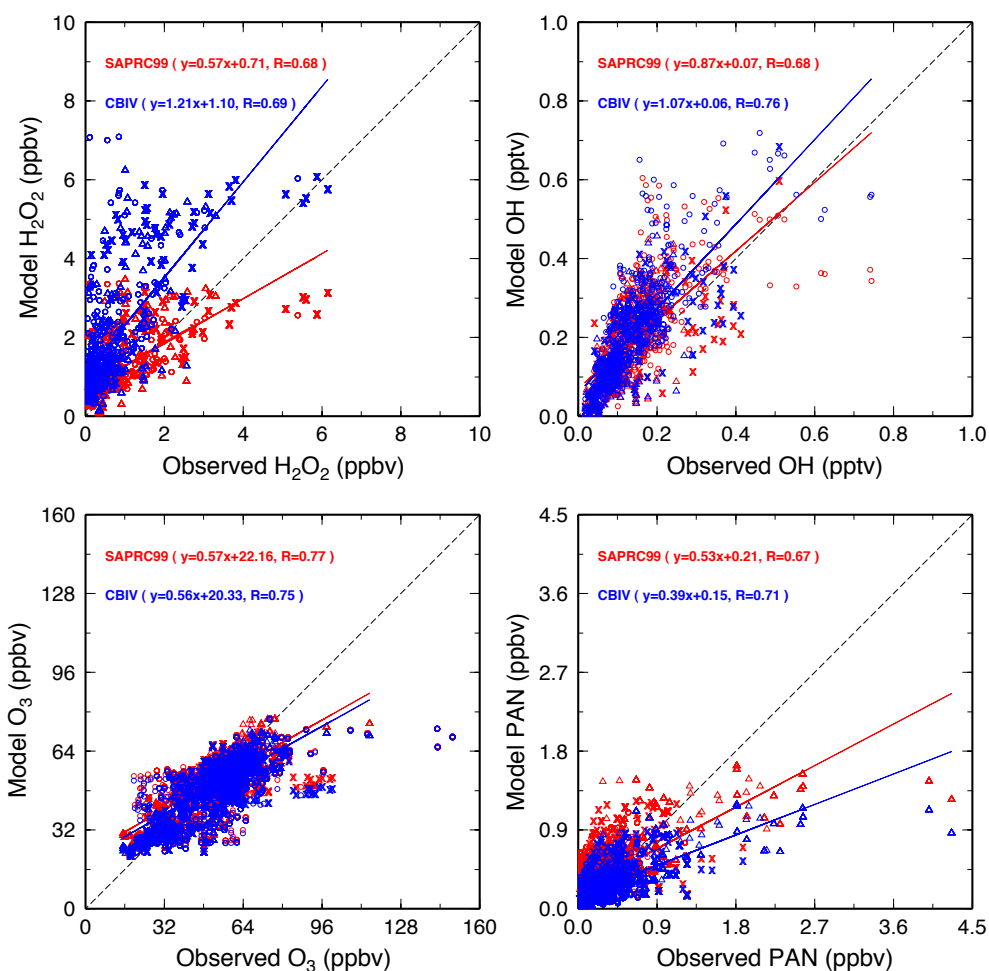
Fig. 10. Comparison of TRACE-P measured and WRF-CMAQ modeled photochemical species with CB4 and SAPRC99 chemistries. Individual points correspond to flight sections at altitudes below 1 km (triangles), 1–3 km (crosses), and above 3 km (circles). Statistics are given for flight sections below 3 km for ozone, and at all altitudes for other chemicals.
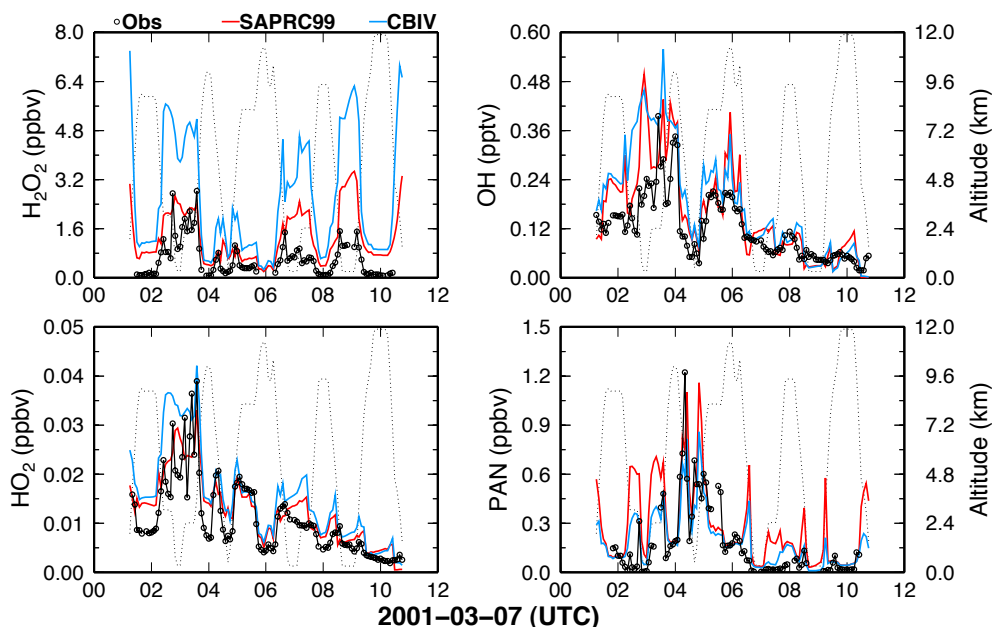
Fig. 11. Comparison of observed and WRF-CMAQ predicted species along the DC-8 flight path on 7 March. The dotted line represents flight altitude (right axis). See Fig. 1b for the flight path.
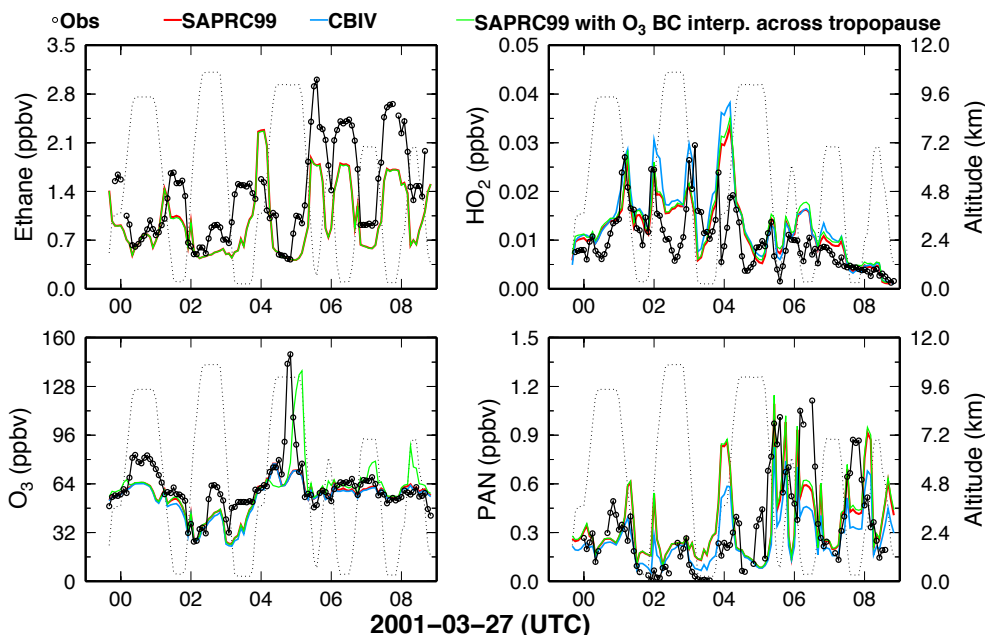
Fig. 12. Comparison of observed and WRF-CMAQ predicted species along the DC-8 flight path on 27 March. See Fig. 1b for the flight path.

the DC-8 flight path on 7 March illustrates that observed and measured PAN distributions clearly show outflow extending to altitudes of 6~8 km as the DC-8 flew through a cold front in the period of 04:00~05:00 UTC. The elevated PAN then serves as a reservoir and carrier of NO_x in the middle and upper troposphere, and may be transported over long distances leading to enhanced O_3 production away from primary NO_x sources by releasing NO_2 when the air masses warm up (Moxim et al., 1996). Compared with all TRACE-P measurements, CB4 shows a correlation of $R=0.71$ and a regression slope of $S=0.39$. SAPRC99 gives a correlation of $R=0.45$ and a regression slope of $S=0.67$. CMAQ captured remarkably well the variation of PAN levels along the flight track. However, both SAPRC99 and

CB4 tends to overpredict low-observed PAN (<0.5 ppbv) at flight altitudes near 3 km (Fig. 11), likely due to errors in the thermal decomposition rate of PAN. SAPRC99 shows somewhat better ability to capture high-observed PAN levels below 1 km with mean bias (*MB*) of −0.05 ppbv in contrast to *MB*=−0.19 ppbv for CB4. This can be traced back to the different treatment of PAN and its analogues in CB4 and SAPRC99. SAPRC99 considers PAN, peroxy propionyl nitrate and other higher alkyl PAN analogues (PAN2), PAN analogues formed from aromatic aldehydes (PBZN), and a PAN analogue formed from methacrolein (MPAN). CB4 considers just the PAN. The rate of PAN decomposition is also higher in SAPRC99 even though the rate of PAN formation is similar between CB4 and SAPRC99.

Hydrogen peroxide (H_2O_2) and the hydroperoxide radical (HO_2) are photochemical products that serve as precursors of odd-oxygen as well as reservoirs of odd-hydrogen radicals. Comparison with TRACE-P measurements reveals that CB4 systematically overpredicts H_2O_2 mixing ratios with a regression slope of $S=1.21$ (Fig. 10). Examination of observed and modeled results along DC-8 flight 7 (Fig. 11) found that CB4 and SAPRC99 give similar predictions at altitudes above 3 km. Below 3 km, however, the overprediction of H_2O_2 in CB4 is up to a factor of 3. The difference in H_2O_2 and HO_2 values are relevant. CMAQ with both mechanisms tracked the observed HO_2 levels remarkably well, and CB4 tends to produce slightly higher HO_2 radicals than SAPRC99. Self-reaction of HO_2 is the only important gas-phase source of H_2O_2 in the troposphere. CB4 uses a 62% higher conversion rate for HO_2 to H_2O_2 reaction than SAPRC99 (Luecken et al., 2007). In consequence, SAPRC99 produces 20–50% less H_2O_2 in summertime over Central Eastern China and downwind areas than CB4. Our analysis for the sringtime suggests that the conversion rate for the HO_2 to H_2O_2 reaction is too high in CB4. Previous sensitivity studies over North America have suggested that SAPRC99 tends to produce higher radical concentrations leading to enhanced O_3 production (e.g. Luecken et al., 2007), but our results show that SAPRC99 produces lower OH and HO_2 radicals in springtime compared with CB4.

The analysis of photochemical sensitivity in this study has demonstrated that the choice of chemical mechanisms can cause a large difference in simulating key oxidants over East Asia. Neither the CB4 nor SAPRC99 mechanisms consistently capture the observed behavior of PAN and H_2O_2 in springtime. Understanding the causes of these differences is needed to give us more confidence, and a better understanding of the uncertainties in current models. Use of detailed mechanisms is necessary for: 1) large releases of precursors, 2) reactivity-based alternative simulations, and 3) multi-day effects. But model results need to be interpreted with care because they may not necessarily be the best representation of the actual processes.

5 Diurnal variation of ground-level ozone

Previous studies examining variations of boundary layer O_3 over East Asia generally used monthly or daily mean data (e.g. Liu et al., 2002; Yamaji et al., 2006). The present section of this study uses hourly data to examine the role of chemistry evolution, vertical mixing and dry deposition processes on diurnal behavior of ground-level O_3. Model results of hourly O_3 and NO_x mixing ratios with five different configurations are compared with EANET measurements taken in Japan (Fig. 13).

5.1 Resolution dependence of chemical processes

The difference between CB4 and SAPRC99 is further examined by comparing both 81-km and 27-km simulations of MM5-CMAQ with hourly measurement data from EANET. Table 3 shows the overall statistics of five model scenarios. Comparison of hourly O_3 predictions between CB4 and SAPRC99 shows an intriguing feature: with 81 km resolution, CB4 systematically improves statistical scores over SAPRC99 in reproducing the magnitude of observed O_3, but with 27 km resolution, SAPRC99 shows a better ability to capture observed 1-h maximums of O_3 mixing ratios. For example, 9–11 July at Sado-seki and some days at Ijira exhibit this phenomena. In general, fine-grid predictions show better agreement against observations than coarse-grid predictions for minimum and maximum O_3 mixing ratios on observed low–O_3 days. For example, during 17–26 July at Sado-seki, the average difference between the 81-km and 27-km simulations of MM5-CMAQ amounts to 40 ppbv. At the Oki site MM5-CMAQ with 27-km resolution (hereafter referred to as MM5-CMAQ/27 km) presents a correlation of $R=0.42$ and $RMSE=15$ ppbv in contrast to $R=0.2$ and $RMSE=23$ ppbv in the MM5-CMAQ/81,km simulation. Examination of hourly mixing ratios reveals that MM5-CMAQ/81km's overprediction of monthly mean O_3 at Oki (Fig. 2b) is primarily due to large biases on low-O_3 days. Increased spatial resolution improves model results regardless of chemical mechanisms. Our results, going from hemispheric-scale (81 km) to regional-scale (27 km), are consistent with Arnold and Dennis (2006) who show similar improvement from regional (32 km) to urban (8 km and 2 km) scales. Since we are using global model BCs and then downscaling the 81 km results to 27 km, the results indicate the important resolution-dependence of physical and chemical processes.

Overall, higher-resolution simulations show better agreement for diurnal variations of O_3 mixing ratios, suggesting clear benefits in predicting boundary layer O_3 over Asia with a high-resolution regional model. Using hourly varying BCs instead of monthly mean values is one of the key reasons why the MM5-CMAQ/27km simulations improve correlations in simulating O_3 variations over the MM5-CMAQ/81km simulations. The WRF-CMAQ simulation at 27 km horizontal scale (hereafter referred to as WRF-CMAQ/27 km) gives the
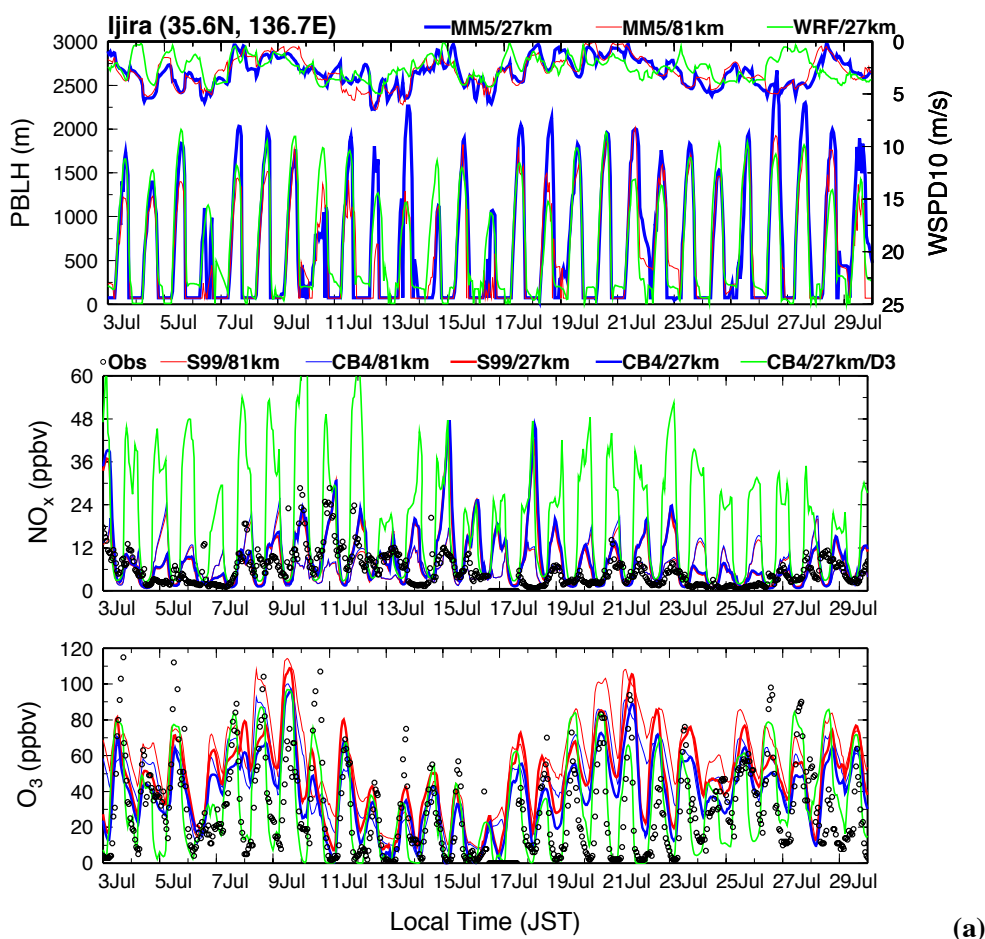
Fig. 13a. Hourly time series of observed and predicted mixing ratios of NO_x and O_3 in July 2001 **(a)** at the rural site Ijira, **(b)** the remote mountain site Happo, **(c)** the remote sites Sado-seki, and **(d)** Yusuhara. The upper panel shows predicted PBL height (left axis) and wind speed at 10 m (right axis).

best statistical scores among five simulations presented. The improvement reflects better resolved meteorological dynamics and land-surface processes in WRF-CMAQ with higher vertical resolution. We will further discuss the impacts of meteorological fields in the next section.

5.2 Boundary layer mixing and local chemistry

Planetary boundary layer (PBL) and land-surface processes have critical implications for air quality simulations. The temporal evolution of O_3 mixing ratios at ground level is controlled strongly by the diurnal variation of the atmospheric boundary layer. This section analyzes the influence of PBL height on O_3 and NO_x mixing ratios, and deposition processes. Variations of ground-level O_3 and NO_x mixing ratios, PBL height and 10 m wind speed on an hourly basis are analyzed for a rural site (Ijira – Fig. 13a), a mountain site (Happo – Fig. 13b), and two remote sites (Sado-seki – Fig. 13c and Yusuhara – Fig. 13d). Observations at urban sites are directly

influenced by local emissions which might not be well represented by the model, thus are not discussed here.

5.2.1 Rural sites

Ijira is a rural EANET site located near the city of Nagoya in central Japan. Intensified diurnal variations of NO_x and O_3 mixing ratios were observed at Ijira (Fig. 13a and Fig. 14). All five simulations generally capture the observed diurnal behavior of O_3 mixing ratios at Ijira, even though the ability to reproduce daytime maximums and nighttime minimums varies. Peak O_3 on several days is in excess of 100 ppbv during the afternoon. Daytime O_3 exceeding 1-h maximums of 70 ppbv occurs on days with wind speeds lower than 3 m/s, suggesting that O_3 at Ijira is mainly formed locally and accumulates in the daytime boundary layer. The correlation R between modeled afternoon O_3 (01:00–03:00 p.m.) and 10 m wind speed from WRF-CMAQ is 0.6. Daytime PBL height plays an essential role in controlling O_3 production at ground level. For example, the lower PBL height shown
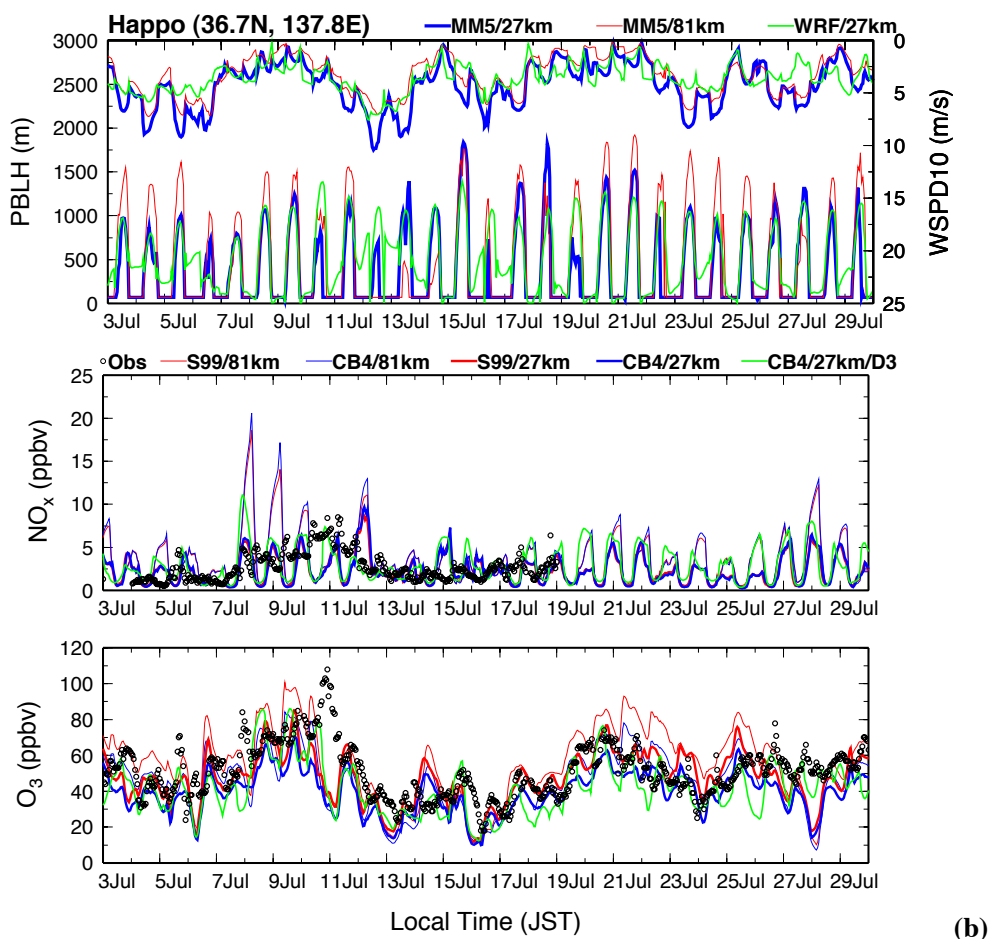
Fig. 13b. Continued.

by the YSU scheme from WRF in part promotes 40 ppbv of daytime O_3 mixing ratios during 26–27 July even though predicted temperature at Ijira from WRF is slightly lower than that from MM5. The decrease in PBL height and wind speed, as well as more concentrated O_3 precursors in the surface layer, explain why WRF-CMAQ/27 km better reproduces observed daytime O_3 maximums during 26–27 July than MM5-CMAQ/27km.

The WRF-CMAQ/27 km simulation significantly improves nighttime O_3 predictions at Ijira. EANET observations represent air pollutants measured a few meters above ground. Thus WRF-CMAQ, with a 17 m deep of surface layer, better represents the observed vertical level. The WRF-CMAQ simulated mixing ratios of O_3 at 180 m are also shown in Fig. 14. The difference in O_3 mixing ratios between the 180-m level and 8-m surface level reveals that the vertical gradient in O_3 mixing ratios reaches its maximum at night. After sunrise, ground-level O_3 becomes equal to that at the 180-m level. This profile suggests that the nighttime accumulation of NO_x in the stable PBL and deposition processes have significant impacts on ground-level O_3 removal at night. Radiative cooling at night leads to the formation of a

stable surface layer near the ground. Above the stable surface layer and under the upper-level inversion, the characteristics of the atmosphere are relatively uniform; this layer is called the nocturnal residual layer. If elevated NO emission sources such as tall industrial smokestacks are not present, O_3 mixing ratios in the residual layer remain high, since deposition and other removal processes that occur near the surface are absent aloft. This can be observed at three remote sites (Fig. 13b–13d). At the rural site Ijira, however, relatively high mixing ratios of NO_x were observed. Thus ground-level O_3 mixing ratios at Ijira decrease after sunset to very low values at nighttime due to NO titration ($NO+O_3 \rightarrow NO_2+O_2$) and deposition processes, and increase dramatically in the morning, reaching a maximum value in the afternoon (01:00–02:00 p.m.). The correlation coefficient between O_3 and NO_x is -0.84 for model results and -0.27 for observations. The negative correlation between O_3 and NO_x suggests that O_3 formation at rural Ijira is in the VOC-limited regime. We find that when nighttime O_3 is depleted by NO_x titration, simulated NO_x levels at night are much higher in WRF-CMAQ than the observed values at Ijira. The major sink of NO_x at night is reaction with O_3 followed by hydrolysis of N_2O_5 on
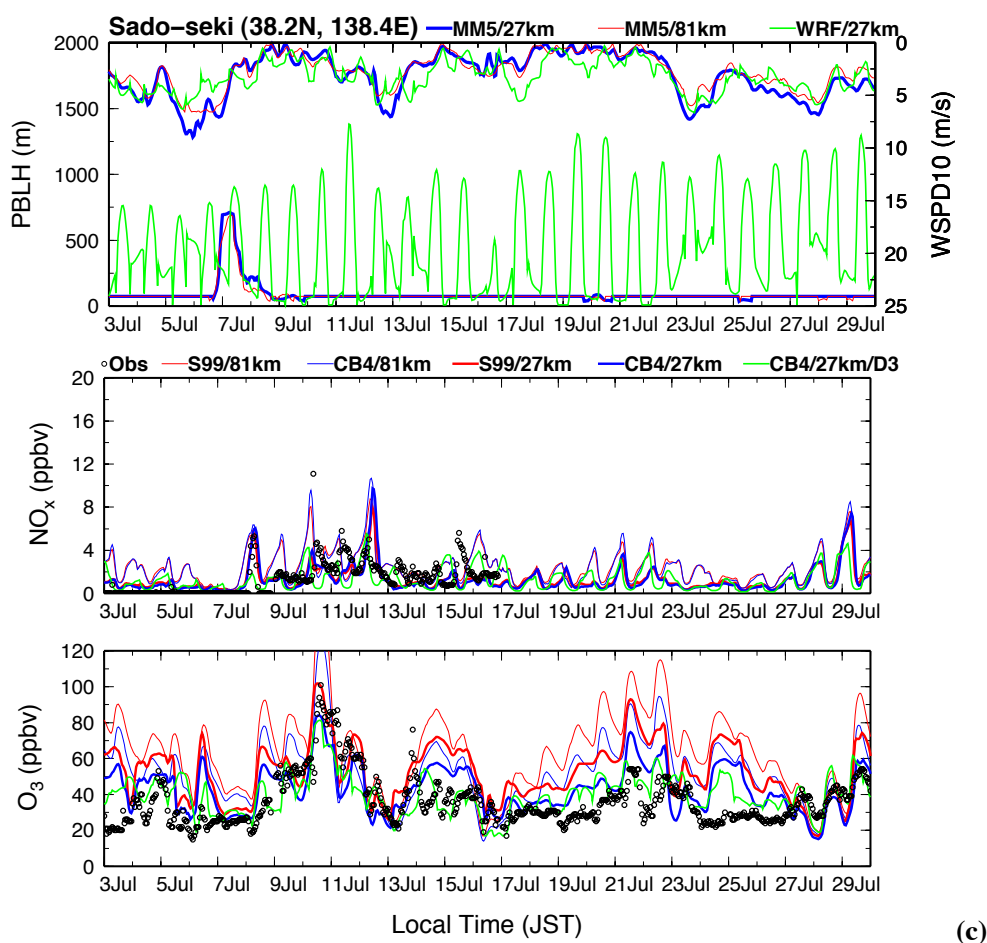
Fig. 13c. Continued.

aerosols. Heterogeneous pathways of N_2O_5 hydrolysis is a weak part of current atmospheric chemistry models. Inadequate treatment of N_2O_5 hydrolysis would in part contribute to the overestimate of nighttime NO_x levels. Another possible cause is the fact that EANET observed aged air masses at Ijira, with most of the emitted NO_x converted to other forms by the time that the air masses were sampled.

The large rate of change in nighttime O_3 among five model simulations clearly illustrates the contribution of NO_x emissions intensity and deposition processes to O_3 destruction at ground level. The artificial dilution of NO_x emissions in the coarse horizontal and/or vertical resolution of MM5-CMAQ results in reduced depletion of O_3 through NO_x titration at night. The intensity of NO_x titration is also influenced by PBL heights and mixing. For example, the difference in nighttime O_3 levels between MM5-CMAQ/81km and MM5-CMAQ/27 km simulations amounts to 40 ppbv during 2–3 July and 21–23 July. During these periods, the MM5/27km PBL height is ∼500 m lower at nighttime, which causes more NO_x to be trapped near the surface and provokes a higher depletion of O_3 in CMAQ. Impacts of PBL heights on O_3 depletion at nighttime can also be examined in the sharp vari-

ations of NO_x mixing ratios on a few days as highlighted in Fig. 14. The correlation between PBL heights and NO_x in the WRF-CMAQ simulation is −0.85. When the PBL height is substantially lower than 250 m, NO_x increases can reach 20 ppbv, which causes the rapid depletion of O_3 at ground level.

The dry deposition flux of O_3 differs considerably between MM5-CMAQ and WRF-CMAQ (Fig. 14). Higher PBL height reflects stronger turbulence and thus may increase dry deposition velocities. For example, the YSU scheme in WRF predicts slightly higher PBL heights at nighttime on 25–26 July than the MRF scheme in MM5, which in part contributes to the increasing dry deposition flux of O_3. Wang et al. (2008) suggested that dry deposition velocity is one of major discrepancies in model simulations for Asia. The parameterization schemes used in current models have been developed and tested using experimental data obtained in North America and Europe, while the deposition processes depend largely on local conditions. Measurements of dry deposition velocities for major air pollutants in Asia would be extremely valuable in the future to improve the parameterizations in model applications for Asia. It would also be valuable to
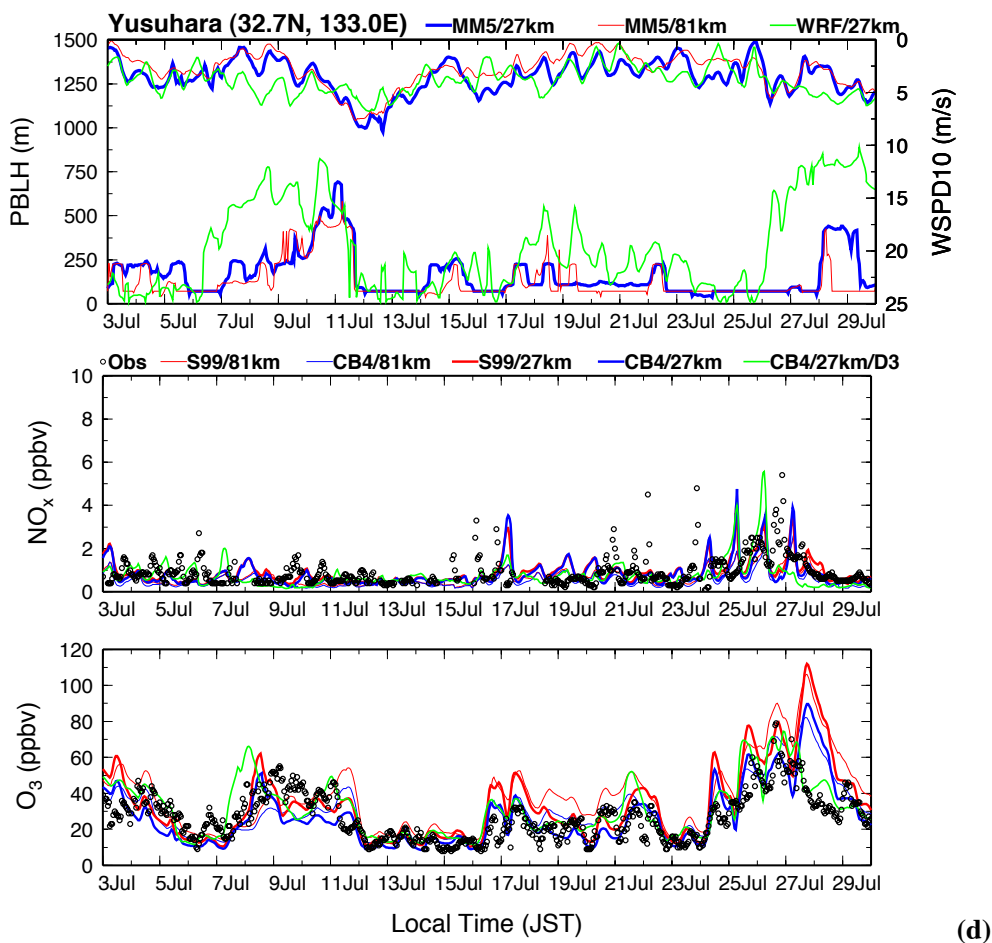
Fig. 13d. Continued.

5.2.2 Remote sites

In contrast to the rural site of Ijira, an obvious diurnal pattern of surface O_3 is not observed at Mt. Happo, Sado-seki or Yusuhara located in relatively clean, remote areas. In remote areas outside the impact of urban pollution plumes, horizontal advection and downward vertical mixing processes are the dominant mechanisms for the build-up of ground-level O_3. All five simulations capture well the day-to-day variability in the observed data at all three remote sites.

Day-to-day variability of daytime O_3 at Happo is shown to have a correlation of $R=0.5$ with changes of surface wind speeds. High O_3 episodes during 7–10 and 19–22 July are correlated with low winds under stagnant conditions. Although a similar diurnal pattern of boundary layer heights is found at Ijira and at Mt. Happo, O_3 mixing ratios at Mt. Happo show little diurnal variation. On 7 and 10 July, the highest observed O_3 mixing ratios are found at midnight, and this behavior is not reproduced by the models. Such behav-

ior is characteristic of mountain stations located above the nocturnal inversion that isolates the site from the effects of surface deposition. The 27-km horizontal scale used in this study is still too coarse to resolve mountain topography and the associated local topographical circulation. The model, due to unrealistic removal of O_3 through dry deposition, generally underestimates nighttime O_3 at Mt. Happo. It would be valuable in the future to examine if a high spatial (1 km) resolution model can reproduce O_3 diurnal behavior at high-altitude sites.

The Sado-seki site is located on Sado island on the west coast of Japan. All model simulations successfully reproduce an elevated-O_3 episode on 10 July associated with stagnant conditions (Fig. 13c). The WRF model predicts large diurnal variations of PBL heights, temperature and latent heat flux reflecting land-surface interactions. Both MM5 simulations predict almost no diurnal variations of these variables. The likely reason for this remarkable difference is that both MM5 81km and 27km grids for Sado-seki are not identified as land in the model. The WRF-CMAQ prediction better reproduces the observed low-O_3 days during 14–22 July at Sado-seki, which greatly improves statistical scores shown in Table. 3.

Table 3. Statistics for hourly mixing ratios of ground-level O_3 in July 2001

Sites	Statistics[a]	SAPRC99/81km MM5-CMAQ	CB4/81 km MM5-CMAQ	SAPRC99/27 km MM5-CMAQ	CB4/27 km MM5-CMAQ	CB4/27 km WRF-CMAQ
Tappi	R	0.43	0.42	0.41	0.41	0.53
	MB	9.6	2.5	2.9	−3.3	−1.9
	RMSE	17.4	11.9	15.4	12.7	11.7
Sado-seki	R	0.43	0.45	0.47	0.50	0.56
	MB	28.3	16.4	17.2	7.3	3.7
	RMSE	34.7	23.3	22.8	14.8	12
Happo	R	0.48	0.48	0.50	0.52	0.58
	MB	4.5	−5.6	−3.4	−11.5	−9.3
	RMSE	18.3	16.6	14.8	17.4	16
Ijira	R	0.43	0.47	0.51	0.56	0.68
	MB	27.1	16.5	18.1	3.3	3.3
	RMSE	38.1	29.6	30	23.9	21.3
Oki	R	0.21	0.19	0.43	0.42	0.43
	MB	27.2	16.6	14.2	5.9	11.1
	RMSE	32.1	22.6	21.2	14.9	18.2
Yusuhara	R	0.64	0.66	0.62	0.62	0.71
	MB	12.3	4.2	8.2	1.0	5.6
	RMSE	19	12.2	17.9	13	12.1

[a] Unit for *MB* and *RMSE* is ppbv.

Evolution of the boundary layer at Yusuhara is quite different from that at the other three sites (Fig. 13d). The PBL height at Yusuhara remains lower than 500 m, except during 7–10 and 25–27 July when O_3 mixing ratios also exhibit higher values than on other days. The positive correlation between ground-level O_3 and PBL height indicates the influence of vertical transport of pollutants aloft down into the surface layer. During 25–27 July, photochemical production, as indicated by high NO_x mixing ratios, partly explains the high levels of surface O_3 in this period. Four MM5-CMAQ simulations systematically overpredict the observed O_3 during 27–28 July, while the WRF-CMAQ prediction reproduces the observed values well. We find that surface wind speed during 27–28 July from WRF is approximately 3 m/s higher than that from MM5, which helps the ventilation of ground-level O_3 at Yusuhara from the boundary layer. The MM5-CMAQ overprediction of O_3 during these two days is likely caused by errors in surface winds from MM5.

6 Conclusions

This study employs the CMAQ regional model to examine spatial and temporal variations of boundary layer O_3 over East Asia. We have evaluated the response of model simula-

tions of boundary layer O_3 and key photochemical oxidants to the choice of chemical mechanisms, meteorological fields, boundary conditions, and model resolutions. Although measurement data are relatively scarce in Asia, we have used available ground-based measurements, aircraft observations obtained from the TRACE-P campaign and satellite data to advance understanding of O_3 chemistry and mechanisms over East Asia and evaluate how well the model represents the observed features.

Boundary conditions of long-lived species exert a great influence on regional model output. Global model BCs tend to provide more realistic spatial and temporal variations of pollution inflow, but might introduce bias as well. We demonstrated that a simple measurement correction of BCs from the MOZART global model systematically improves CMAQ performance near the domain boundaries. Correcting zonal flux with vertical profiles from ozonesonde stations worldwide is recommended for future studies. Regional modelers should choose a global chemistry model driven with assimilated meteorology. In the future, we would benefit from optimal global chemistry model results with the assimilation of large-scale satellite observations of chemical species. Future development in regional models needs to strengthen the coupling between global and regional models, in particular, the treatment of top boundary conditions.
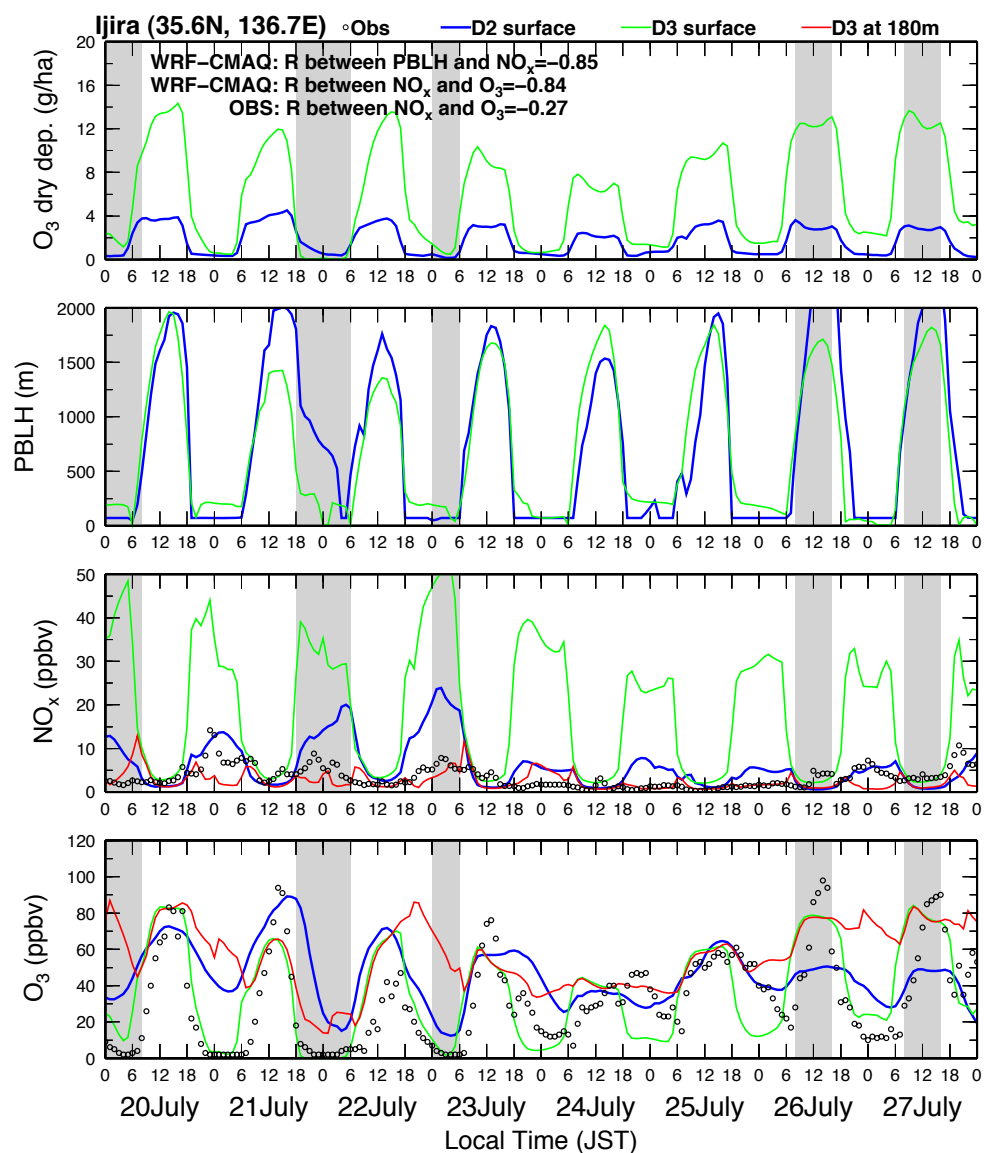
Fig. 14. Diurnal variations of O_3, NO_x, PBL height, and dry deposition at the rural site Ijira during 20–27 July 2001. Episodes with large impacts of PBL height on O_3 mixing ratios are highlighted in gray.

Surface O_3 over East Asia exhibits a latitudinal difference in the seasonal amplitude between the spring maximum and summer minimum in response to the spatially varying influence of the Asian monsoon. The model successfully reproduces the seasonal cycle of surface O_3 at Japanese island sites at lower-latitudes, but tends to underpredict the June maximum and overpredict the August minimum at inland Chinese sites. TRMM satellite measurements and model simulations of summertime rainfall are used to assess the impacts of the Asian monsoon on O_3 production. Our results suggest that summertime O_3 over Central Eastern China is highly sensitive to cloud cover and monsoonal rainfall over this region. Both MM5 using 81 km resolution, and WRF using 27 km resolution, could not accurately simulate the

strong monsoon rainfall over Central Eastern China in July and August, even though WRF somewhat better reproduces both the magnitude and spatial variation of rainfall over most areas. Meteorological model underestimates of cloud cover and rainfall over Central Eastern China in July and August explain why CMAQ tends to overpredict observed O_3 over Beijing during the same period. Thus, accurate simulation of the East Asia summer monsoon is critical to model analysis of atmospheric chemistry over China. Our analysis suggests that meteorological models should be reinitialized every five to ten days with high-quality reanalysis data to maximize consistency with observed weather patterns.

Examination of hourly summertime O_3 mixing ratios from sites in Japan confirms the important role of diurnal boundary layer fluctuations in controlling ground-level O_3. By comparing five different model configurations with observations at six sites, the specific mechanisms responsible for model behavior are identified and discussed. In particular, vertical mixing, NO_x titration, and dry deposition depending on PBL height strongly affect model ability to capture observed behavior. Lower PBL height enhances the build-up of ground-level O_3 during daytime, but causes a more complete depletion of O_3 by NO_x titration at night. A large vertical gradient of boundary layer O_3 is found over rural and urban areas. Our analysis demonstrates clear benefits of using a high-resolution model in evaluating transport and chemical transformation of Asian pollutants. The WRF-CMAQ simulation using 27 km horizontal scale and 29 vertical layers gives the best statistical scores in evaluating the day-to-day and diurnal variations of ground-level O_3. Future studies should ensure that model vertical resolution is adequate to resolve near surface chemical processes and land-surface interactions. Surface layer depth less than 20 m is recommended to better represent measured conditions of ground-based stations.

Central Eastern China appears to be the most sensitive region in our study to the choice of chemical mechanisms. Evaluation with TRACE-P aircraft measurements reveals that neither the CB4 nor the SAPRC99 mechanisms consistently capture observed behavior of key photochemical oxidants in springtime. However, our analysis finds that SAPRC99 performs somewhat better in simulating mixing ratios of H_2O_2 and PAN at flight altitudes below 1 km. The CB4 mechanism overpredicts H_2O_2 by a factor of two, which is caused by higher self-reaction rates of HO_2. SAPRC99 predicts 50% higher PAN, because more PAN analogues and a lower decomposition rate of PAN are considered in SAPRC99 than in CB4. The overall higher load of VOC, explicit organic peroxy radicals, and inclusion of radical recycling processes explain why SAPRC99 predicts 10–20 ppbv higher O_3 during summertime for Central Eastern China and downwind areas. Our findings suggest that future model studies over this region should carefully examine chemistry sensitivities, especially in regulatory applications – such as the design of emission control policies. Between CB4 and SAPRC99, the more detailed SAPRC99 mechanism is suggested for future studies examining high-O_3 episodes, the impacts of large releases of precursors, and multi-day effects.

Improvements of regional atmospheric chemistry models will require efforts in reducing uncertainty in emissions, meteorology, photochemistry, and global pollution inflow. The high level of uncertainty associated with O_3 production in Central Eastern China poses a major problem for regional air quality management. This highly polluted, densely populated region would greatly benefit from comprehensive air quality monitoring and the development of model chemical mechanisms appropriate to this unique atmospheric environment.

References

Arnold, J. and Dennis, R. L.: Testing CMAQ chemistry sensitivities in base case and emissions control runs at SEARCH and SOS99 surface sites in the southeastern US, Atmos. Environ., 40, 5027–5040, doi:10.1016/j.atmosenv.2005.05.055, 2006.

Byun, D. W. and Ching, J. K. S. (Eds.): Science algorithms of the EPA models-3 community multi-scale air quality (CMAQ) modeling system, NERL, Research Triangle Park, NC, USA, 1999.

Byun, D. W. and Schere, K. L.: Review of the governing equations, computational algorithms, and other components of the Models-3 Community Multiscale Air Quality (CMAQ) modeling system, Appl. Mech. Rev., 59, 51–77, 2006.

Carmichael, G. R., Ferm, M., and Thongboonchoo, N., et al.: Measurements of sulfur dioxide, ozone and ammonia concentrations in Asia, Africa, and South America using passive samplers, Atmos. Environ., 37, 1293–1308, doi:10.1016/S1352-2310(02)01009-9, 2003a.

Carmichael, G. R., Tang, Y., and Kurata, G., et al.: Evaluating regional emission estimates using the TRACE-P observations, J. Geophys. Res. 108(D21), 8810, doi:10.1029/2002JD003116, 2003b.

Carmichael, G. R., Tang, Y. and Kurata, G. et al.: Regional-scale chemical transport modeling in support of the analysis of observations obtained during the TRACE-P experiment. J. Geophys. Res. 108(D21), 8823, doi:10.1029/2002JD003117, 2003c.

Carter, W.: Implementation of the saprc-99 chemical mechanism into the models-3 framework. Report to the United States Environmental Protection Agency, 29 January, 2000.

Ding, A. and Wang, T.: Influence of stratosphere-to-troposphere exchange on the seasonal cycle of surface ozone at Mount Waliguan in western China. Geophys. Res. Lett., 33(3), 1–4, doi:10.1029/2005GL024760, 2006.

Ding, A. J., Wang, T., Thouret, V., Cammas, J.-P., Nédélec, P.: Tropospheric ozone climatology over Beijing: analysis of aircraft data from the MOZAIC program, Atmos. Chem. Phys., 8(1), 1–13, 2008.

EANET: Data Report on the Acid Deposition in the East Asian Region, 2001–2007, available at: http://www.eanet.cc/product.html, Network Center for EANET, 2008.

Fan, J. W., Zhang, R. Y., Li, G. H., Nielsen-Gammon, J., and Li, Z. Q. Simulations of fine particulate matter (PM2.5) in Houston, Texas, J. Geophys. Res., 110, D16203, doi:10.1029/2005JD005805, 2005.

Faraji, M., Kimura, Y., McDonald-Buller, E., and Allen, D.: Comparison of the carbon bond and SAPRC photochemical mechanisms under conditions relevant to southeast texas, Atmos. Env-

iron., 42 (23), 5821–5836, doi:10.1016/j.atmosenv.2007.07.048, 2008.

Fiore, A. M., Dentener, F. and Wild, O., et al.: Muti-model estimates of intercontinental source-receptor relationships for ozone pollution. J. Geophys. Res., 114, D04301, doi:10.1029/2008JD010816, 2008.

Fishman, J., Ramanathan, V., Crutzen, P. J., and Liu, S. C.: Tropospheric ozone and climate, Nature 282, 818–820, 1979.

Fu, T.-M., Jacob, D. J., Palmer, P. I., Chance, K., Wang, Y. X., Barletta, B., Blake, D. R., Stanton, J. C., and Pilling, M. J.: Space-based formaldehyde measurements as constraints on volatile organic compound emissions in east and south Asia and implications for ozone, J. Geophys. Res. 112, D06312, doi:10.1029/2006JD007853, 2007.

Gery, M., Whitten, G. Z., Killus, J. P., and Dodge, M. C.: A photochemical kinetics mechanism for urban and regional scale computer modeling. J. Geophys. Res. 94 (D10), 12925–12956, 1989.

Guenther, A., Karl, T., Harley, P., Wiedinmyer, C., Palmer, P. I., and Geron, C.: Estimates of global terrestrial isoprene emissions using megan (model of emissions of gases and aerosols from nature), Atmos. Chem. Phys., 6(11), 3181–3210, 2006.

Han Z., Sakurai T., and Ueda H. et al.: MICS-Asia II: Model intercomparison and evaluation of ozone and relevant species, Atmos. Environ., 42(15), 3491–3509, doi:10.1016/j.atmosenv.2007.07.031, 2007.

He, Y. J., Uno, I., Wang, Z. F., Pochanart, P., Li, J., and Akimoto, H.: Significant impact of the east asia monsoon on ozone seasonal behavior in the boundary layer of eastern china and the west pacific region, Atmos. Chem. Phys., 8(4), 14927–14955, http://www.atmos-chem-phys.net/8/7543/2008/, 2008.

Holloway T., Sakurai, T., and Han, Z., et al. MICS-Asia II: Impacts of global emissions on regional air quality in Asia, Atmos. Environ., 42(15), 3543–3561, doi:10.1016/j.atmosenv.2007.10.022, 2007.

Horowitz, L. W., Walters, S., Mauzerall, D. L., Emmons, L. K., Rasch, P. J., Granier, C., Tie, X. X., Lamarque, J. F., Schultz, M. G., Tyndall, G. S., Orlando, J. J., and Brasseur, G. P.: A global simulation of tropospheric ozone and related tracers: Description and evaluation of MOZART, version 2, J. Geophys. Res., 108(D24), 4784, doi:10.1029/2002JD002853, 2003.

Huffman, G. J., Adler, R. F., Bolvin, D. T., Gu, G., Nelkin, E. J., Bowman, K. P., Hong, Y., Stocker, E. F., and Wolff, D. B.: The TRMM multi-satellite precipitation analysis: Quasi-global, multi-year, combined-sensor precipitation estimates at fine scale, J. Hydrometeor., 8(1), 38–55, 2007.

Jacob, D. J.: Introduction to Atmospheric Chemistry. Princeton University Press, Princeton, New Jersey, USA, 231–232, 1999.

Jacob, D. J., Crawford, J. H., Kleb, M. M., Connors, V. S., Bendura, R. J., Raper, J. L., Sachse, G. W., Gille, J. C., Emmons, L., and Heald, C. L.: Transport and Chemical Evolution over the Pacific (TRACE-P) aircraft mission: Design, execution, and first results, J. Geophys. Res. 108(D20), 1–19, doi:10.1029/2002JD003726, 2003.

Kim, J., Lee, H., and Lee, S.: The characteristics of tropospheric ozone seasonality observed from ozone soundings at Pohang, Korea, Environ. Monitor. Assess., 118, 1–12, 2006.

Lee, E., Chase, T. N., and Rajagopalan, B.: Seasonal forcasting of East Asian summer monsoon based on oceanic heat sources, Int. J. Climatol., 28, 667–678, 2008.

Lefer, B. L., Shetter, R. E., Hall, S. R., Crawford, J. H., and Olson, J. R. Impact of clouds and aerosols on photolysis frequencies and photochemistry during TRACE-P: 1. analysis using radiative transfer and photochemical box models, J. Geophys. Res., 108(D2), 8821, doi:10.1029/2002JD003171, 2003.

Li, J., Wang, Z., Akimoto, H., Gao, C., Pochanart, P., and Wang, X.: Modeling study of ozone seasonal cycle in lower troposphere over east Asia, J. Geophys. Res., 112, D22S25, doi:10.1029/2006JD008209, 2007.

Lin, M., Oki, T., Holloway, T., Streets, D. G., Bengtsson, M., and Kanae, S.: Long-range transport of acidifying substances in East Asia – Part I: Model evaluation and sensitivity studies, Atmos. Environ., 42(24), 5939–5955, doi:10.1016/j.atmosenv.2008.04.008, 2008a.

Lin, M., Oki, T., Bengtsson, M., Kanae, S., Holloway, T., and Streets, D. G.: Long-range transport of acidifying substances in Asia – Part II: Source-receptor relationships, Atmos. Environ., 42(24), 5956–5967, doi:10.1016/j.atmosenv.2008.03.039, 2008b.

Lin, W., Xu, X., Zhang, X., Tang, J.: Contributions of pollutants from North China Plain to surface ozone at the Shangdianzi GAW station, Atmos. Chem. Phys., 8, 5889–5898, 2008c.

Liu, H., Crawfordi, J. H., and Pierce, R. B. et al.: Radiative effect of clouds on tropospheric chemistry in a global three-dimensional chemical transport model, J. Geophys. Res., 111, D20303, doi:10.1029/2005JD006403, 2006.

Liu, H. Y., Jacob, D. J., Chan, L. Y., Oltmans, S. J., Bey, I., Yantosca, R. M., Harris, J. M., Duncan, B. N., Martin, R. V. Sources of tropospheric ozone along the Asian Pacific Rim: An analysis of ozonesonde observations, J. Geophys. Res. 107(D21), 4573, doi:10.1029/2001JD002005, 2002.

Luecken, D. J., Phillips, S., Sarwar, G., and Jang, C.: Effects of using the CB05 vs. SAPRC99 vs. CB4 chemical mechanism on model predictions: Ozone and gas-phase photochemical precursor concentrations, Atmos. Environ., 42(23), doi:10.1016/j.atmosenv.2007.08.056, 2007.

Ma, J., Zheng, X., and Xu, X.: Comment on "Why does surface ozone peak in summertime at Waliguan?" Zhu, B., Akimoto, H., and Wang, Z., et al., Geophys. Res. Lett. 32, L01805, doi:10.1029/2004GL021683, 2005.

Ma, J., Zhou, X., and Hauglustaine, D.: Summertime tropospheric ozone over China simulated with a regional chemical transport model, 2. source contributions and budget, J. Geophys. Res., 107(D22), 4612, doi:10.1029/2001JD001355, 2002.

Moxim II, W. J., H. L., and Kasibhatla, P. S.: Simulated global tropospheric PAN: Its transport and impact on NO_x. J. Geophys. Res., 101(D7), 12621–12638., 1996.

Naja, M. and Akimoto, H. :Contribution of regional pollution and long-range transport to the Asia-Pacific region: Analysis of long-term ozonesonde data over Japan, J. Geophys. Res., 109, D21306, doi:10.1029/2004JD004687, 2004.

Richter, A., Burrows, J. P., Nuss, H., Granier, C., and Niemeier, U. Increase in tropospheric nitrogen dioxide over China observed from space, Nature, 437(7055), 129–132, 2005.

Sarwar, G., Luecken, D., Yarwood, G., Whitten, G., Carter, W.: Impact of an updated carbon bond mechanism on predictions from the community multiscale air quality modeling system: preliminary assessment, J. Appl. Meteorol. Climatol., 47(1), 3–14, doi:10.1175/2007JAMC1393.1, 2008.

Streets, D. G., Bond, T. C., Carmichael, G. R., Fernandes, S. D., Fu, Q., He, D., Klimont, Z., Nelson, S. M., Tsai, N. Y., Wang, M. Q., Woo, J. H., and Yarber, K. F.: An inventory of gaseous and primary aerosol emissions in Asia in the year 2000. J. Geophys. Res., 108(D21), 8809, doi:10.1029/2002JD003093, 2003.

Tang Y. and Carmichael, G. R. and Thongboonchoo, N. et al.: Influence of lateral and top boundary conditions on regional air quality prediction: A multiscale study coupling regional and global chemical transport models, J. Geophys. Res., 112, D10S18, doi:10.1029/2006JD007515, 2007.

van der Werf, G. R., Randerson, J. T., Giglio, L., Collatz, G. J., Kasibhatla, P. S., and Arellano, A. F.: Interannual variability in global biomass burning emissions from 1997 to 2004, Atmos. Chem. Phys., 6, 3423–3441, 2006,
http://www.atmos-chem-phys.net/6/3423/2006/.

Wang, Y., McElroy, M. B., Munger, J. W., Hao, J., Ma, H., Nielsen, C. P., and Chen, Y.: Variations of O_3 and CO in summertime at a rural site near beijing, Atmos. Chem. Phys., 8(21), 6355–6363, 2008.

Wang, Z., Li, J., Wang, X., Pochanart, P., and Akimoto, H.: Modeling of regional high ozone episode observed at two mountain sites (Mt. Tai and Huang) in east China, J. Atmos. Chem., 55, 253–272, 2006.

Wang, Z., Xie, F., and Sakurai, T., et al.: MICS-ASIA II: Model inter-comparison and evaluation of acid deposition. Atmos. Environ., 42(15), 3528–3542, doi:10.1016/j.atmosenv.2007.12.071, 2008.

Xu, X., Lin, W., Wang, T., Yan, P., Tang, J., Meng, Z., and Wang, Y.: Long-term trend of surface ozone at a regional background station in eastern China 1991–2006: enhanced variability, Atmos. Chem. Phys., 8(10), 2595–2607, 2008.

Yamaji, K., Ohara, T., Uno, I., Tanimoto, H., Kurokawa, J., and Akimoto, H.: Analysis of the seasonal variation of ozone in the boundary layer in East Asia using the Community Multiscale Air Quality model: What controls surface ozone levels over Japan?, Atmos. Environ., 40(10), 1856–1868, 2006.

Yarwood, G., Stoeckenius, T. E., Heiken, J. G., and Dunker, A. M.: Modeling weekday/weekend ozone differences in the Los Angeles region for 1997, J. Air Waste Manage. Assoc., 53, 864–875, 2003.

Zaveri, R. A. and Peters, L. K. A new lumped structure photochemical mechanism for large-scale applications, J. Geophys. Res., 104(D23), 30387–30415, 1999.

Zhang M. G., Uno, I., Carmichael, G. R., et al.: Large-scale structure of trace gas and aerosol distributions over the western Pacific Ocean during the Transport and Chemical Evolution Over the Pacific (TRACE-P) experiment, J. Geophys. Res., 108(D21), doi:10.1029/2002JD002946, 2003.

Zhao, C., Wang, Y., and Zeng, T.: East china plains: A "basin" of ozone pollution, Environ. Sci. Technol., 43(6), 1911–1915, 2009.

Zhu, B., Akimoto, H., Wang, Z., Sudo, K., Tang, J., and Uno, I. Why does surface ozone peak in summertime at Waliguan?, Geophys. Res. Lett., 31(17), 1–4, doi:10.1029/2004GL020609, 2004.